Summer 8-2019

QUANTUM CHEMICAL CALCULATIONS APPLIED TO SOMO-HOMO CONVERSION AND VIBRATIONALLY AVERAGED NMR SHIELDING PARAMETERS

Erik Johnson
University of Nebraska - Lincoln, johnson.erik@huskers.unl.edu

QUANTUM CHEMICAL CALCULATIONS APPLIED TO SOMO-HOMO CONVERSION AND VIBRATIONALLY AVERAGED NMR SHIELDING PARAMETERS

by

Erik C. Johnson

A THESIS

Presented to the Faculty of

The Graduate College at the University of Nebraska

In Partial Fulfillment of Requirements

For the Degree of Master of Science

Major: Chemistry

Under the Supervision of Professor Gerard S. Harbison

August, 2019

QUANTUM CHEMICAL CALCULATIONS APPLIED TO SOMO-HOMO CONVERSION AND VIBRATIONALLY AVERAGED NMR SHIELDING PARAMETERS

Erik Charles Johnson, M.S.

University of Nebraska, 2019

Advisor: Gerard S. Harbison

The inversion of frontier orbitals of free radicals was studied using density functional theory calculations in Gaussian 09. Comparisons of images of orbitals in GaussView was used to assess the relative positions of singly occupied and doubly occupied orbitals and to determine which was the highest in energy. A variety of organic free radicals were studied including several radical anions and also a neutral radical. It was found that cross-conjugation appears to be a factor in whether or not molecules show SOMO-HOMO conversion. Cross-conjugation is when two unsaturated groups are conjugated to a third unsaturated group but are not conjugated to each other.

Formaldehyde was analyzed by vibrational self-consistent field (VSCF) calculations at two different levels of theory, Hartree-Fock (HF) and Möller-Plesset 2nd-Order Perturbation Theory (MP2). The calculations were repeated using three different basis sets, aug-cc-pVnZ, n = 2 − 4. Convergence was observed for the VSCF-PT2 (MP2) frequencies for each of the six normal modes of vibration as the basis set was expanded. There was also good agreement

between VSCF-PT2 calculated frequencies and experimental values for frequencies of the modes. The chemical shielding constants were calculated using NMR calculations based on the coordinates at 16 different displacements along the vibrational motions for each of the modes. The average chemical shielding values for each mode were determined using the chemical shielding values at the 16 different displacements from equilibrium and the values of the wavefunctions of the modes of vibration at each different displacement. Another NMR calculation was performed for formaldehyde in its optimized conformation, and then the chemical shielding difference from equilibrium across all the modes was calculated for each atom. The differences were added to the equilibrium chemical shielding values to yield vibrationally corrected chemical shielding values. Corrected shielding constants calculated with basis sets aug-cc-pVTZ and aug-cc-pVQZ were close to experiment. In addition, ethylene and methane were analyzed by VSCF and vibrationally corrected chemical shielding values were calculated for these molecules.

Acknowledgements

Professor Andrzej Rajca, my advisor for the project on SOMO-HOMO conversion

Professor Gerard Harbison, my advisor for the project on VSCF and chemical shielding

Petroleum Research Fund Grant Number 56195-ND6 was a critical source of funding in 2018.

I certify that all of the work described within this thesis is the original work of the author. Any published (or unpublished) ideas and/or techniques from the work of others are fully acknowledged in accordance with standard referencing practices.

Erik C. Johnson

August 1, 2019

Introduction

First, I will be discussing SOMO-HOMO conversion of organic radicals.

SOMO-HOMO conversion has to do with relative energies of molecular orbitals in free radicals. The orbital which contains the unpaired electron in a free radical may be the highest energy occupied molecular orbital or it may be lower in energy than the highest energy occupied molecular orbital. Radicals of the latter type are called SOMO-HOMO converted radicals. This is of significance for stability of free radicals since if the orbital containing an unpaired electron has an energy lesser than that of a doubly occupied molecular orbital then when one electron is removed from the free radical, the resultant molecule is still a free radical, in this case a diradical. Alternatively, when one electron is added to such a converted free radical, similarly it is likely that the electron would be added to the lowest unoccupied molecular orbital thus forming a diradical. Stable free radicals have some usefulness in various fields including spin-labeling for magnetic resonance imaging. There is interest in designing high-spin polyradicals which could be of usefulness for their interesting magnetic properties. Molecular electronic devices can be fashioned from such high-spin polyradicals.

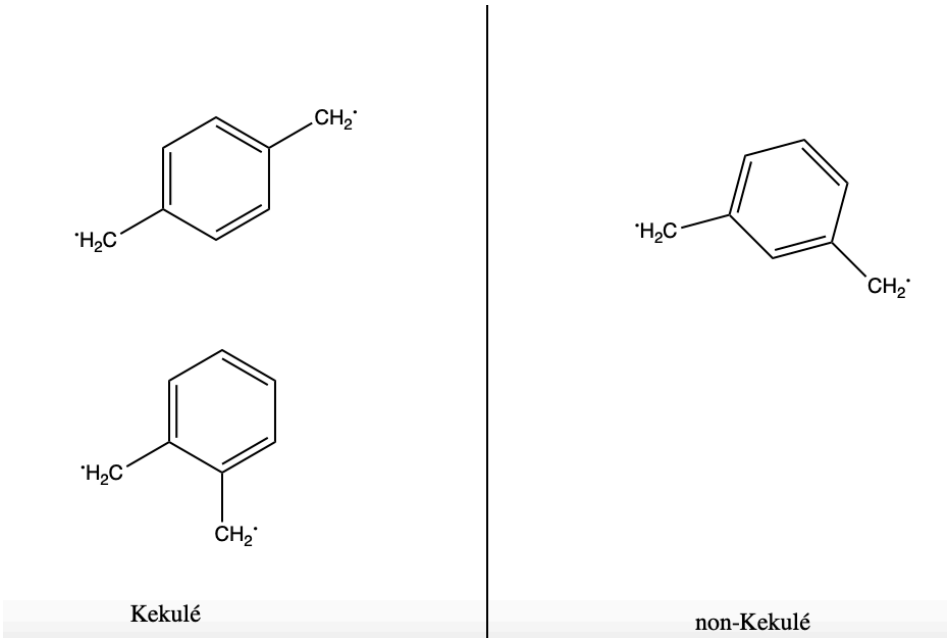

Figure 1: Diagram of Kekulé and of non-Kekulé diradicals.

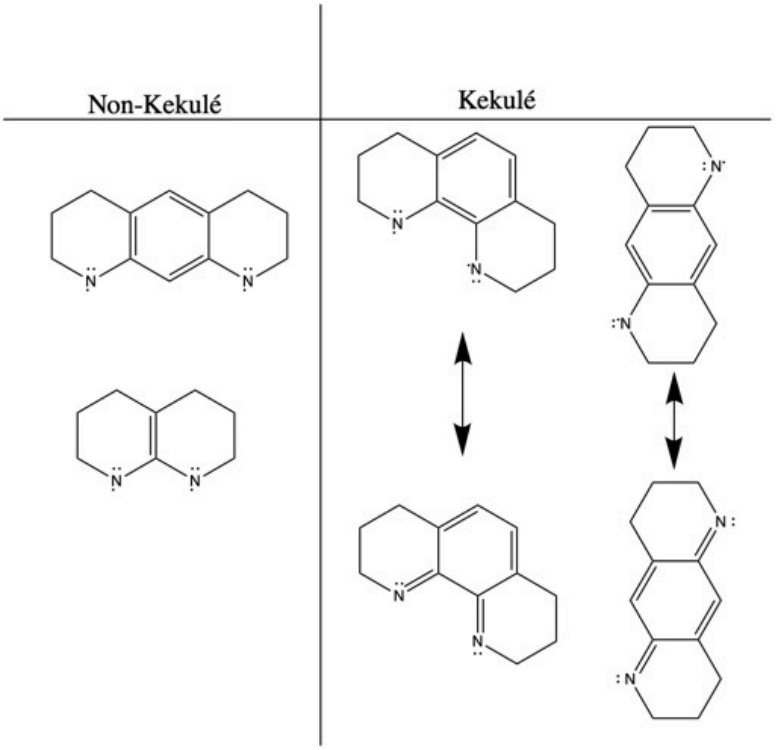

Figure 2: Examples of Kekulé and of non-Kekulé structures analyzed for whether or not they show SOMO-HOMO conversion in their anionic forms.

Kekulé and non-Kekulé free radicals are of significance in this study. Non-Kekulé structures in general contain at least two atoms that are not pi-conjugated. In non-Kekulé-type diradicals, while the unpaired electrons are adjacent to the pi-conjugated system, there does not exist a resonance structure such that all of the electrons of the molecule are paired. For a Kekulé-type diradical, there exists a resonance structure such that all electrons are paired. The singlet-triplet energy gaps of non-Kekulé nitrogen-rich acene diradicals appear to be lesser than the singlet-triplet energy gaps of nitrogen-rich Kekulé-type acene diradicals. [1] This may be especially relevant in correlation of SOMO-HOMO energy gaps of converted radicals with singlet-triplet energy gaps of the diradical forms of the converted radical structures. Out of the structures studied in this work, all of the structures that showed conversion were non-Kekulé in their diradical forms, where diradical form refers to the molecule generated by one-electron oxidation of the monoradical.

Also arguably of significance in this study is something called cross-conjugation. Cross-conjugation is when two unsaturated groups are both conjugated to a third unsaturated group but are not conjugated to each other. Out of the structures investigated, all that show conversion are cross-conjugated, but, not all cross-conjugated structures show conversion.

Second, I will be discussing calculation of NMR shielding parameters of some organic molecules and how they are affected by vibrations of a molecule in each of its normal modes of vibration. Chemical shielding has to do with the magnetic environment occupied by a nucleus, and chemical shift of a nucleus is found by comparing the chemical shielding of one nucleus to that of a reference nucleus. Various factors determine the amount of chemical shielding. These include the electrons that surround a nucleus and their electron correlation, the neighboring nuclei, and interactions of the magnetic dipoles of nuclear spins with each other. Also the interactions of the nuclei with the external applied magnetic fields of the NMR spectrometer impact chemical shielding. The applied magnetic fields include both the main applied magnetic field of the spectrometer magnet and the radiofrequency pulses used in the NMR experiment. The method used to calculate the shielding constants is 2nd-order Möller-Plesset perturbation theory (MP2), and coordinates from vibrational self-consistent field (VSCF) computations of the normal modes are used as input. Coordinates at several points along the vibrational motion of each normal mode are given as input.

[1] S. Amiri; P. R. Schreiner, Non-Kekulé *N*-Substituted *m*-Phenylenes: *N*-Centered Diradicals versus Zwitterions, J. Phys. Chem. A 113 (2009) 11750–11757.

Chapter 1.
SOMO-HOMO Conversion.

Abstract.

The inversion of frontier orbitals of free radicals was studied using density functional theory calculations. Comparisons of images of orbitals in GaussView was used to assess the relative positions of singly occupied and doubly occupied orbitals and to determine which was the highest in energy. A variety of organic free radicals were studied including several radical anions and also a neutral radical. It was found that cross-conjugation appears to be a factor in whether or not molecules show SOMO-HOMO conversion. Cross-conjugation is when two unsaturated groups are conjugated to a third unsaturated group but are not conjugated to each other. Also Koopmans' Theorem, which states that the HOMO energy is equal to the negative of the ionization potential, appears to have some relevance in the correlation of the SOMO-HOMO energy gaps for radical anions and the singlet-triplet energy gaps of the corresponding diradicals formed by removal of a single electron from the radical anions.

Introduction

SOMO-HOMO conversion, also known as SOMO-HOMO inversion, is when the highest doubly occupied molecular orbital (HDMO) of a radical is higher in energy than the singly occupied molecular orbital (SOMO) of the radical. SOMO-HOMO conversion has been observed in some distonic radical anions, meaning radical anions where the radical and anion components are not connected to each other by a π system.[1] (Figures 1.1 and 1.2). Another example of SOMO-HOMO conversion is seen in DNA base pairs as shown in the following two figures.[2] Figures 1.3 and 1.4.

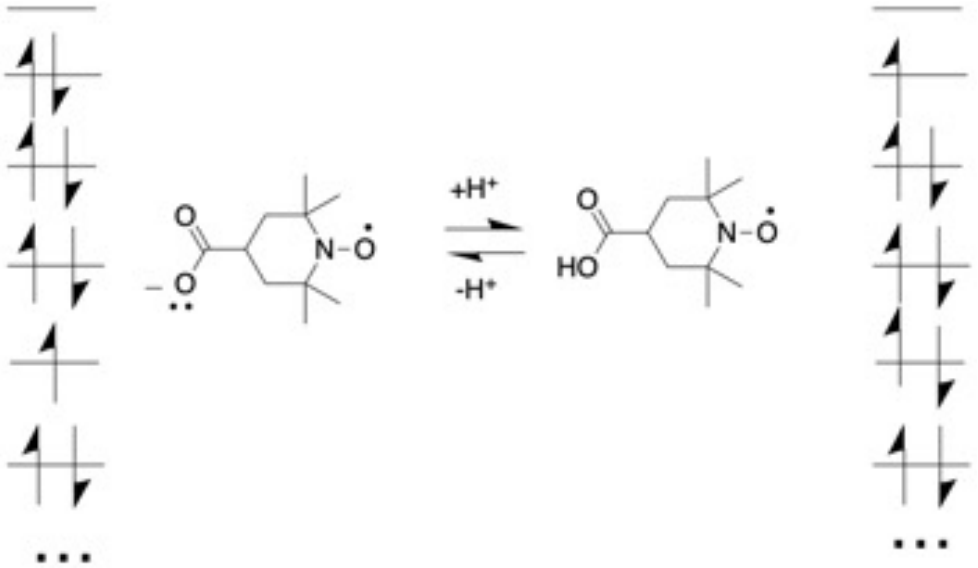

Figure 1.2: SOMO-HOMO converted radical anion in equilibrium with non-converted neutral radical. [1]

Studying SOMO-HOMO conversion may be useful for designing stable organic radicals including high-spin polyradicals that could be used for building purely organic nanoscale magnetic devices. Stable free radicals can be useful as spin labels for magnetic

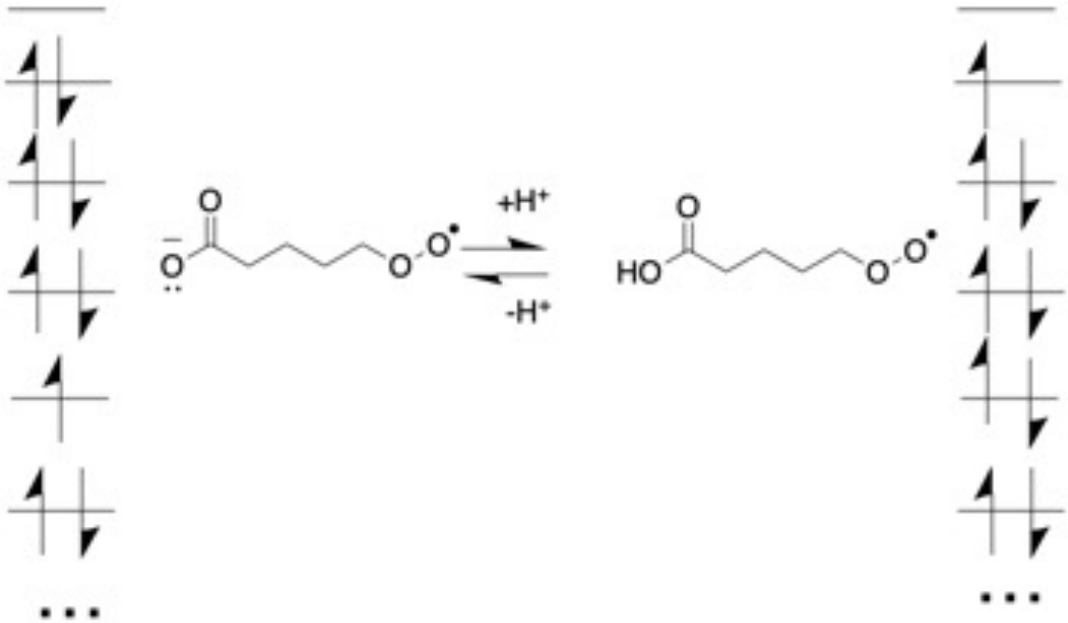

Figure 1.1: SOMO-HOMO converted radical anion in equilibrium with non-converted neutral radical. [1]

resonance imaging. Polymers of organic radicals could have high spin and potentially show spintronics properties which are useful in a variety of applications.

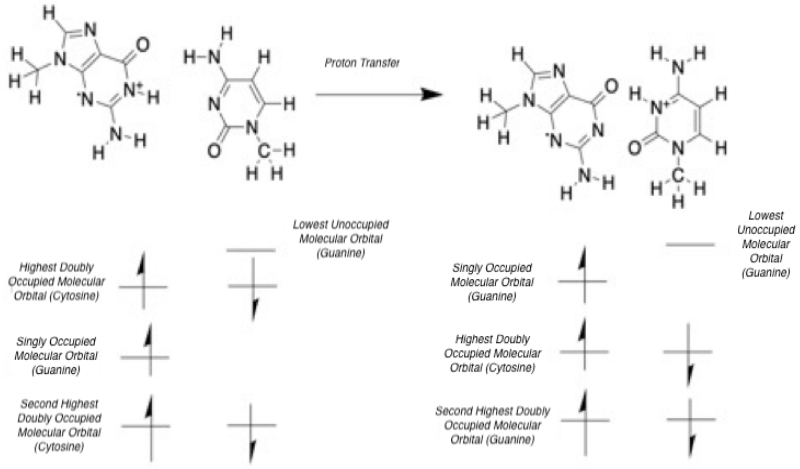

Figure 1.4: SOMO-HOMO converted Guanine-Cytosine base pair and one-proton transfer to form nonconverted base pair. [2]

Research Questions and Methods

Density Functional Theory calculations were performed using GAUSSIAN 09 to determine whether SOMO-HOMO conversion occurs in some organic radical anions. The molecules studied were organic radicals that were not too large, containing around

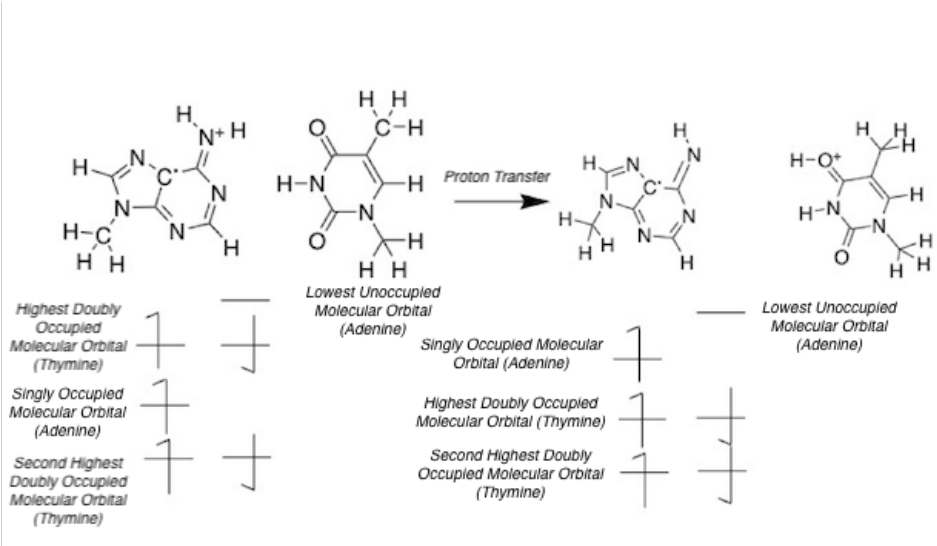

Figure 1.3: SOMO-HOMO converted Adenine-Thymine base pair and one-proton transfer to form nonconverted base pair. [2]

eight to fourteen carbon atoms each, with a few containing several more. Many of the structures studied were substituted with some heteroatoms including nitrogen, oxygen, and phosphorus. Some of the structures computed are shown in Figure 1.5. All structures computed had the radical component and the anion or electron-rich component connected to each other by a π system. Some structures were conjugated and others were cross-conjugated. "A cross-conjugated compound may be defined as a compound possessing three unsaturated groups, two of which although conjugated to a third unsaturated center are not conjugated to each other." Conjugated means connected by a system of alternating double and single bonds.[3]

One research question explored was: how do conjugation and cross-conjugation affect SOMO-HOMO conversion? A second research question explored was: what is the relationship, if any, between the HOMO-SOMO energy gap for the radical anion or monoradical and the singlet-triplet energy gap for the corresponding diradical formed by removing a single electron from the radical anion or monoradical? The diradical forms of the molecules which were formed by removing a single electron from the highest doubly occupied molecular orbital of each radical anion were also optimized and their frequencies computed. Both triplet and singlet states of these diradicals were computed. The singlet states were computed using the broken-symmetry DFT (BS-DFT) method. The calculations were performed using the GAUSSIAN 09 program and included unrestricted B3LYP (UB3LYP) and unrestricted M06-2X (UM06-2X). The basis sets used were 6-31+G(d,p) for anions and 6-31G(d,p) for neutral molecules and cations. The singlet-triplet energy gaps were computed and plotted against the difference in energy between the alpha highest doubly occupied orbital and the alpha highest singly occupied orbital for the corresponding radical anion from which the diradical was formed by removal of an electron. The orbital energies of the anion and singlet-triplet gap of the diradical were also computed in a solvent of water using the Polarized Continuum Model of solvation (PCM) with the Self-Consistent Reaction Field (SCRF) keyword in GAUSSIAN.

UM06-2X was used in addition to UB3LYP because UB3LYP suffers from self-interaction errors but UM06-2X does not and thus may be more accurate in computing energies of the orbitals of ionized forms of these molecules such as the radical anions.

The singlet-triplet energy gaps are obtained by subtracting the energy of the triplet state from the energy of the singlet state and then multiplying by a correction factor that involves the squares of the spin angular momenta for the two states. The correction factor is needed because the broken-symmetry DFT method, which was used to compute the geometries of the singlet states, may not be very accurate.

The formula for the singlet-triplet energy gap, ΔE_{ST} is:

$$\Delta E_{ST} = (E_S - E_T) \cdot \left(\frac{S_T^2}{S_T^2 - S_S^2} \right)$$

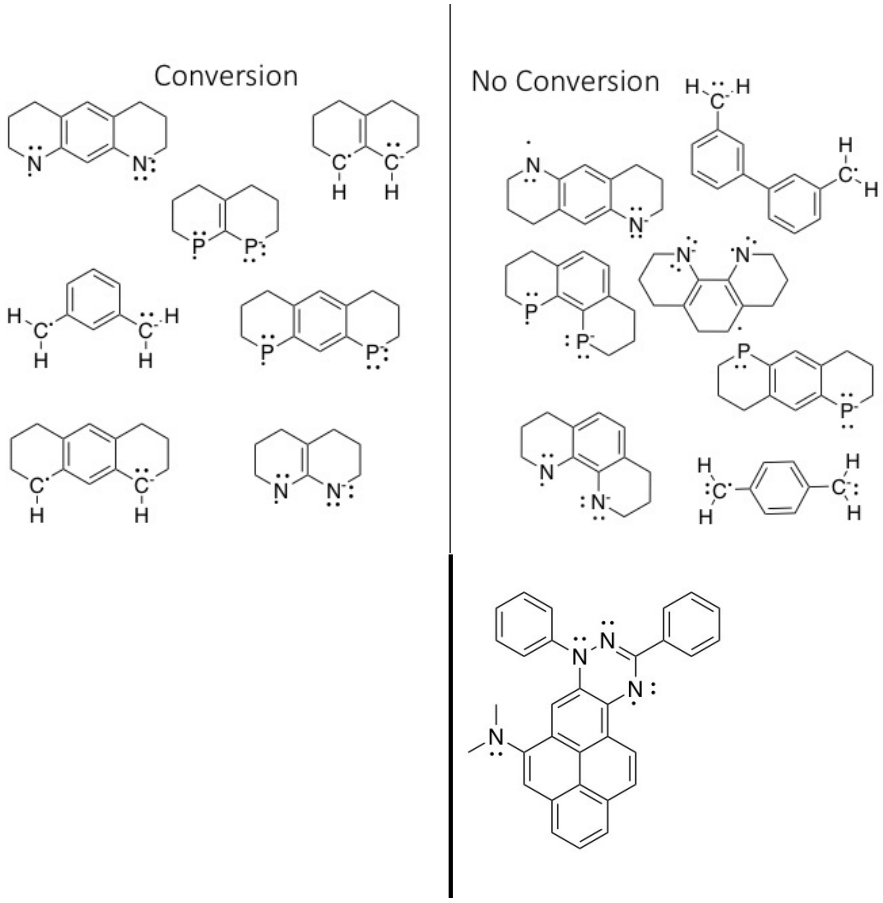

Figure 1.5: Structures considered for whether or not they show SOMO-HOMO conversion.

Results and Discussion

A linear correlation between singlet-triplet energy gaps and HOMO-SOMO energy gaps was observed both in gas phase and in water, as shown in Figures 1.6-1.9. This may be accounted for by Koopmans' approximation or Koopmans' theorem, which states that "the ionization potential required to remove an electron from the orbital Ψ_i is given by the negative value of the energy of the orbital, $-\varepsilon_i$, as calculated within the Hartree-Fock approximation."[4] Whether a singlet or a triplet is formed from the radical anion in an ionization event is determined by the direction of the spin of the electron that is removed. Koopmans' theorem can tell us that highest occupied molecular orbital energies are "frozen" so that when one electron is removed from a highest doubly occupied molecular orbital, the energy of the orbital remains constant. Orbital relaxation can be neglected in making the energy comparisons; therefore the difference in energy of one-electron ionization for the two electrons in the highest doubly occupied molecular orbital is equal to the singlet-triplet energy gap.

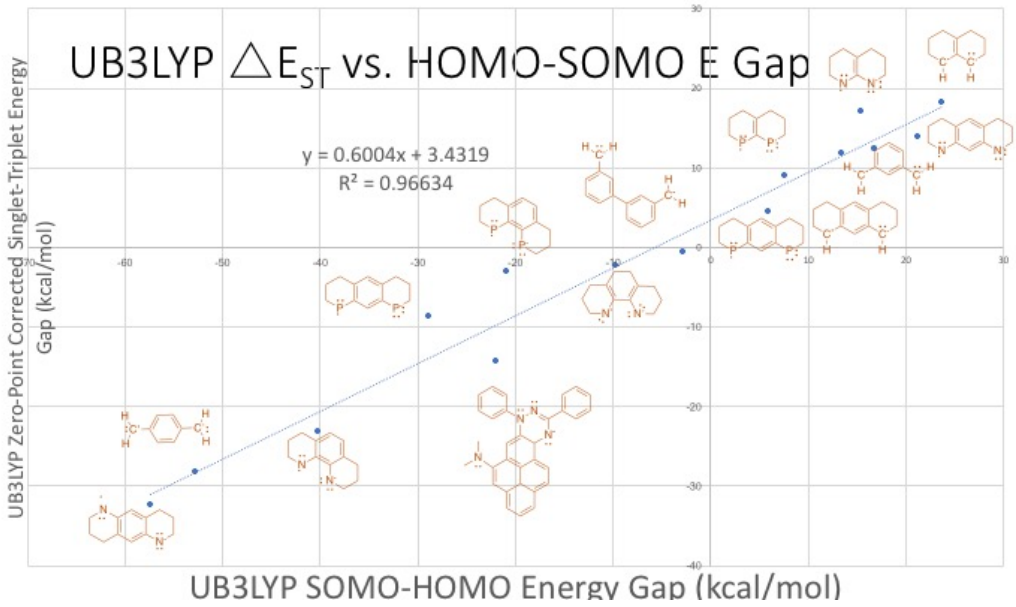

Figure 1.6: UB3LYP Singlet-Triplet Gap for Diradicals versus HOMO-SOMO Energy Gap for Radical Anions.

Koopmans' Approximation can explain not only the linear correlation between HOMO energy and ionization potential, but, by extension, can explain a linear correlation between the HOMO-SOMO energy gap and the singlet-triplet energy gap.

Table 1.1 shows the r squared values and slopes of the plots and Figure 1.10 shows orbital configurations for a one-electron oxidation event.

While not all cross-conjugated structures show conversion, so far all structures that show conversion are cross-conjugated. Figure 1.11 shows two structures that, while cross-conjugated, do not show conversion.

Future Work

In the future I will need to perform stable optimization calculations on all the results to test if the wavefunction is a stable minimum or not for each optimization. Also I will do some MP2 calculations on the same structures already computed using DFT in order to yield more accurate energy levels and more accurate singlet-triplet gaps than can be obtained from DFT. Also I will probably do some multireference calculations on these molecules which may include Complete Active Space SCF (CASSCF) and

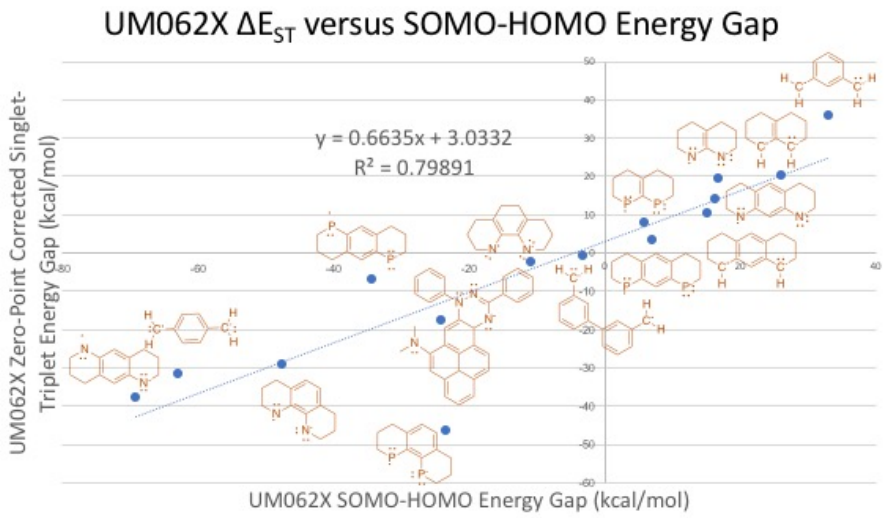

Figure 1.7: UM06-2X Singlet-Triplet Gap for Diradicals versus HOMO-SOMO Energy Gap for Radical Anions.

Configuration Interaction (CI) calculations. These multireference calculations, which sample different electron configurations, may yield more accurate singlet-triplet energy gaps for the diradical forms of these molecules.

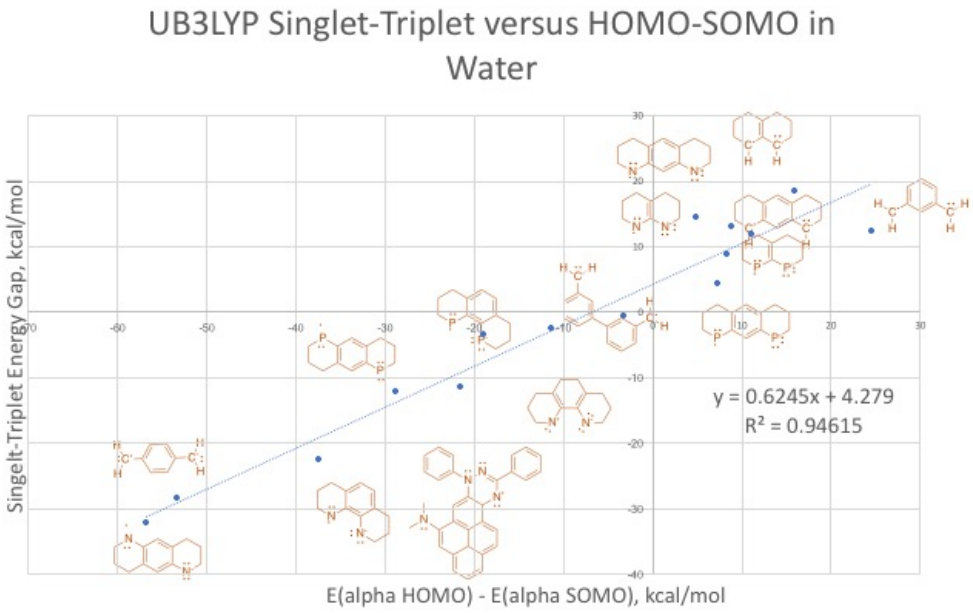

Figure 1.8: UB3LYP Singlet-Triplet Gap for Diradicals in water versus HOMO-SOMO Energy Gap for Radical Anions in water.

In addition, it is possible in the future that I will compute the energy difference between ferromagnetic and antiferromagnetic states of an organic radical polymer, the ferromagnetic state being one in which all the spins of the unpaired electrons are aligned, the antiferromagnetic state being one in which spins of unpaired electrons point in opposite directions for adjacent units of the polymer.

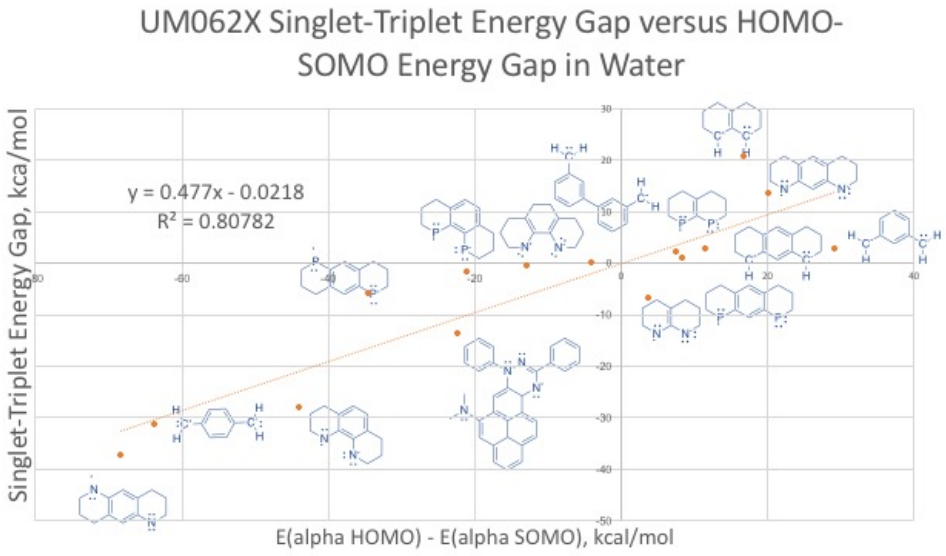

Figure 1.9: UM06-2X Singlet-Triplet Gap for Diradicals in water versus HOMO-SOMO Energy Gap for Radical Anions in water.

Table 1.1: Slopes and R values of linear fits for UB3LYP and UM06-2X calculations either in gas phase or in water.

Calculation	Solvent	Slope	R^2 Value
UB3LYP	Gas Phase	0.6004	0.96634
UM06-2X	Gas Phase	0.6635	0.79891
UP3LYP	Water	0.6245	0.94615
UM06-2X	Water	0.477	0.80782

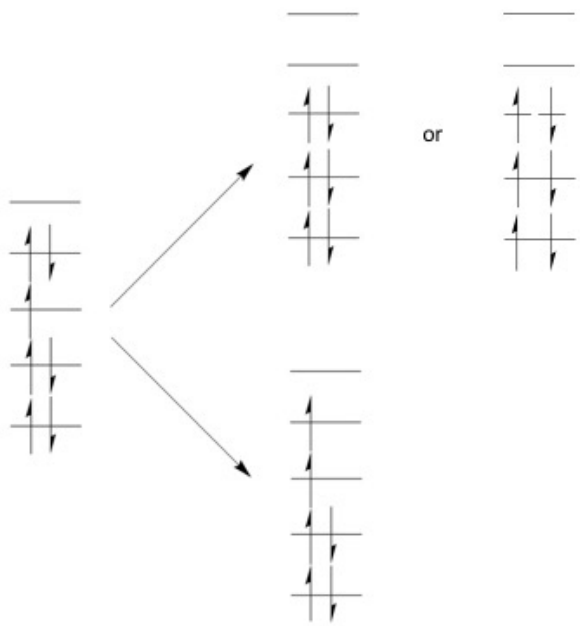

Figure 1.10: Formation of either a triplet or a singlet state by a one-electron ionization of a SOMO-HOMO converted radical.

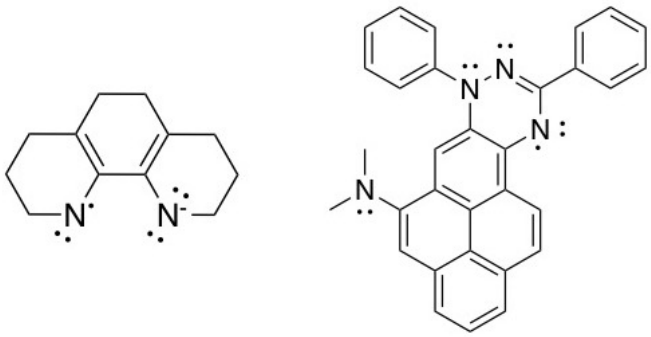

Figure 1.11: Two structures that are cross-conjugated but do not show conversion.

References

[1] M. L. Coote, G. Gryn'ova, D. L. Marshall, S.J. Blanksby, Switching radical stability by pH-induced orbital conversion, Nature Chemistry 5 (2013) 474-481.

[2] A. Kumar, M. D. Sevilla, Proton transfer induced SOMO-to-HOMO level switching in one-electron oxidized A-T and G-C base pairs: a density functional theory study, J. Phys. Chem. B 118 (2014) 5453-5458.

[3] N. F. Phelan, M. Orchin, Cross conjugation, J. Chem. Education 45 (1968) 633-637.

[4] V. I. Minkin, Glossary Of Terms Used In Theoretical Organic Chemistry, Pure Appl. Chem. 71 (1999) 1919 – 1981. (Page 1949.)

Chapter 2.
Vibrational Self-Consistent Field Calculations

Abstract

Formaldehyde was analyzed by vibrational self-consistent field (VSCF) calculations at two different levels of theory, Hartree-Fock (HF) and Möller-Plesset 2nd-Order Perturbation Theory (MP2). The calculations were repeated using three different basis sets, aug-cc-pV*n*Z, $n = 2 - 4$. Convergence was observed for the VSCF-PT2 (MP2) frequencies for each of the six normal modes of vibration as the basis set was expanded. There was also good agreement between VSCF-PT2 calculated frequencies and experimental values for frequencies of the modes. The chemical shielding constants were calculated using NMR calculations based on the coordinates at 16 different displacements along the vibrational motions for each of the modes. The average chemical shielding values for each mode were determined using the chemical shielding values at the 16 different displacements from equilibrium and the values of the wavefunctions of the modes of vibration at each different displacement. Another NMR calculation was

performed for formaldehyde in its optimized conformation, and then the chemical shielding difference from equilibrium across all the modes was calculated for each atom. The differences were added to the equilibrium chemical shielding values to yield vibrationally corrected chemical shielding values. Oxygen had the highest magnitude of chemical shielding differences from equilibrium, followed by carbon, and hydrogen had the lowest in magnitude chemical shielding differences from equilibrium. Corrected shielding constants calculated with basis sets aug-cc-pVTZ and aug-cc-pVQZ were close to experiment. In addition, ethylene and methane were analyzed by VSCF and vibrationally corrected chemical shielding values were calculated for these molecules.

Introduction

Vibrational spectroscopy includes infrared (IR) spectroscopy and Raman spectroscopy. Vibrational modes are IR-active if the dipole moment of the molecule changes during the vibrational motion. Vibrational modes are Raman active if the polarizability of the molecule changes during the vibrational motion.

Molecular vibrations can be modeled by a harmonic oscillator. A harmonic oscillator is a physical model that is based on a mass vibrating on a spring. An example of a harmonic oscillator is a mass attached to one end of a spring that is fixed at the other end. The stiffness of the spring is described by k,the spring constant. The restoring force acting on the mass at a displacement x from the equilibrium position is $F = -kx$. Using Newton's second law, where force equals mass times acceleration, we can write [1,2]:

$$m\frac{d^2x}{dt^2} = -kx \qquad (2.1)$$

Equation (1) can be solved for position as a function of time, momentum as a function of time, and frequency.

The solutions are [2]:

$$x(t) = Asin(\omega t)p(t) = m\omega Acos(\omega t)\omega = (k/m)^{1/2} \qquad (2.2)$$

The potential energy of the system is based on the displacement of the mass from equilibrium or, alternatively, the difference between the spring length at time t and the equilibrium spring length. While the total energy is constant throughout the motion, the potential energy equals $\frac{1}{2}kx^2$. In the harmonic approximation, the potential energy curve for a harmonic oscillator is a parabola with a minimum at the equilibrium position. The greater the spring constant k,the steeper are the walls of the parabola. The harmonic oscillator can be used to model the vibrations of a diatomic molecule or of a polyatomic molecule with more than two atoms. For a real diatomic molecule, the bond vibration may not follow the harmonic approximation because at great interatomic separation the atoms dissociate and so the energy plateaus rather than going up to infinity at large values

of bond distance r. The energy would still go up to infinity as the interatomic distance r decreases to zero due to Coulombic repulsion of the nuclei. This is modeled by the Morse potential which is discussed later, as illustrated in Figure 2.1. The deviation from the harmonic approximation for a real diatomic molecule is known as anharmonicity.

An equation for describing the potential energy of a diatomic molecule is the following:[3]

$$U_0(r) = U(r = r_e) + (r - r_e)\frac{dU}{dr}|_{(r=r_e)} + \frac{1}{2}(r - r_e)^2\frac{d^2U}{dr^2}|_{(r=r_e)} + 3^{rd}order + - - - \quad (2.3)$$

For the harmonic approximation, only second order and lower terms are included; for anharmonicity, terms of third order or higher must also be included in addition to the lower terms.

In the harmonic approximation, the vibrational energy levels of a diatomic molecule are determined by solving the Schrödinger equation and the solution as a function of the vibrational quantum number v and the fundamental frequency of vibration $\tilde{\nu}$, where the frequency is expressed in wavenumbers, is:

$$\tilde{G}(v) = (v + \tfrac{1}{2})\tilde{\nu} \qquad \tilde{\nu} = \frac{1}{2\pi c}\left(\frac{k_f}{m_{eff}}\right)^{1/2} \quad (2.4)$$

An example of an expression for potential energy of an oscillator that includes anharmonicity is the Morse potential.

The Morse potential energy is given by:

$$V = hc\tilde{D}_e\{1 - e^{-a(R-R_e)}\}^2 a = \left(\frac{m_{eff}\omega^2}{2hc\tilde{D}_e}\right)^{1/2} \quad (2.5)$$

$\tilde{D}_e$ is the depth of the potential well. Figure 2.1 shows the Morse potential for N_2 in its ground

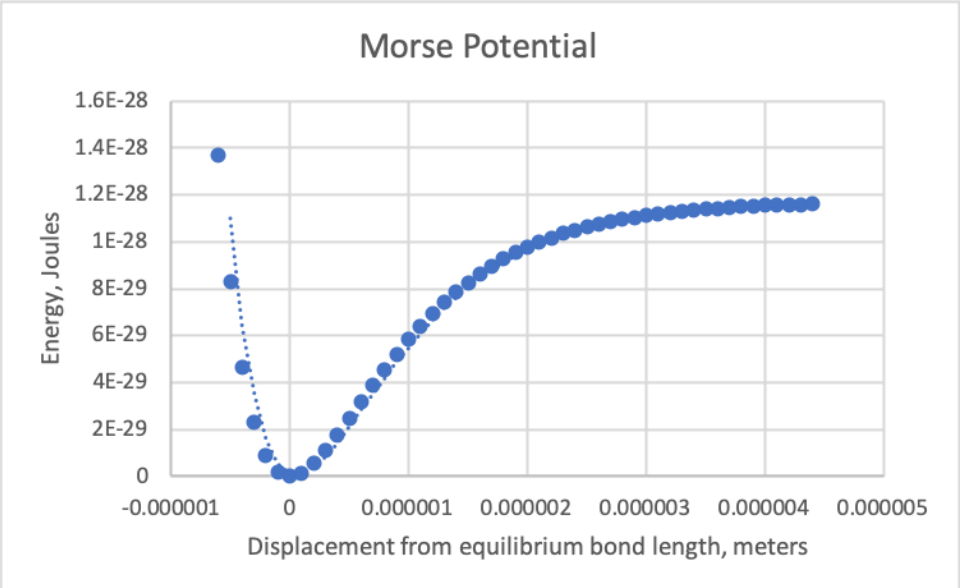

Figure 2.1: Morse Potential for N_2 in its ground electronic state.

electronic state.

Solving the Schrödinger equation for the Morse potential yields the following expression for the energy levels:

$$\tilde{G}(v) = (v + \frac{1}{2})\tilde{\nu} - (v + \frac{1}{2})^2 x_e \tilde{\nu} x_e = \frac{a^2 \hbar}{2 m_{eff} \omega} = \frac{\tilde{\nu}}{4 D_e} \qquad (2.6)$$

A Morse oscillator has a finite number of vibrational energy levels, and the spacing between successive vibrational energy levels v and $v + 1$ decreases as the quantum number v increases.

A normal mode of vibration is defined as follows. The equation

$$q_i = A_i cos(\lambda^{1/2} t + \epsilon) \qquad (2.7)$$

is one solution of a differential equation that describes a molecule modeled as a harmonic oscillator. [4]

For a polyatomic molecule containing N atoms, the $3N$ differential equations

$$\ddot{q}_j + \sum_{i=1}^{3N} f_{ij} q_j = 0, j = 1,2, \ldots, 3N \qquad (2.8)$$

describe the motion of the atoms. $\ddot{q}$ is the second time derivative of the variable q.

$$f_{ij} = \left(\frac{\partial^2 V}{\partial q_i \partial q_j} \right)_0 \qquad (2.9)$$

Equation 2.7 is a solution for these equations. λ, ϵ, and A_i are constants; A_i is the amplitude, λ the wavelength, and ϵ the phase. Substituting Eq. 2.7 into Eq. 2.8 yields:

$$\sum_{i=1}^{3N} (f_{ij} - \delta_{ij} \lambda) A_i = 0 j = 1,2, \ldots, 3N \qquad (2.10)$$

where $\delta_{ij} = 1$ if $i = j, \delta_{ij} = 0$ if $i \neq j$.

Other than the trivial solution $A_i = 0$ for all i, the only solutions of Eq. 2.8 use values of λ satisfying the equation:

$$\begin{vmatrix} f_{11} - \lambda & f_{12} & f_{13} & \cdots & f_{1,3N} \\ f_{21} & f_{22} - \lambda & f_{23} & \cdots & f_{2,3N} \\ \cdots & \cdots & \cdots & \cdots & \cdots \\ f_{(3N,1)} & f_{(3N,2)} & f_{(3N,3)} & \cdots & f_{(3N,3N)} - \lambda \end{vmatrix} = 0$$

(2.11)

known as the secular equation. The vertical lines in this equation indicate the determinant of the matrix in between them. A particular non-trivial solution of this equation may be denoted by λ_k. Such a solution λ_k specifies exact values of the coefficients of A_i in Equation 2.8. Then it is possible to reach a solution for specific values of the A_i's, and the A_i associated with a certain λ_k are called A_{ik}. One specific λ_k does not give unique values for the A_{ik}'s but only gives the ratios of the A_{ik}'s. Setting $A_{1k} = 1$ results in an arbitrary set of A_{ik}'s which may be called A'_{ik}. It is possible to specify a unique mathematical solution to the system of equations Equations 2.10, called l_{ik}, based on such an arbitrary set A'_{ik}:

$$l_{ik} = \frac{A'_{ik}}{[\sum_i (A'_{ik})^2]^{\frac{1}{2}}} \qquad (2.12)$$

The amplitudes are normalized:

$$\sum_i l_{ik}^2 = 1 \qquad (2.13)$$

Setting

$$A_{ik} = K_k l_{ik} \qquad (2.14)$$

solves the problem. The K_k are constants that are based on the initial values of the coordinates q_i and velocities $\dot{q}_i$. $\dot{q}_i$ is the first time derivative of q_i.

The matrix in Equation 2.11 has $3N$ rows and $3N$ columns, one row and one column for each of the unknown A_is.
For nonlinear molecules the secular equation has $3N - 6$ nonzero roots. For linear molecules the secular equation has $3N - 5$ nonzero roots.

"Each atom is oscillating about its equilibrium position with a simple harmonic motion of amplitude $A_{ik} = K_k l_{ik}$, frequency $\frac{\lambda^{1/2}}{2\pi}$, and phase ϵ_k. Corresponding to a given solution λ_k of the secular equation, the frequency and phase of the motion of each coordinate is the same, but the amplitudes may be, and usually are, different for each coordinate. On account of the equality of phase and frequency, each atom reaches its position of maximum displacement at the same time, and each atom passes through its equilibrium position at the same time. A mode of vibration having all these characteristics is called a *normal mode of vibration,* and its frequency is known as a *normal,* or *fundamental frequency* of the molecule." [4]

This project involves vibrational SCF (VSCF) which involves solving the vibrational Schrödinger equation.[5] VSCF yields a vibrational wavefunction for each of the normal modes of the molecule. Self-Consistent Field (SCF) calculations in VSCF involve a method analogous to the Hartree Self-Consistent Field Method, which is a variational method where a trial variation function is introduced to model atomic orbitals. In the Hartree SCF method, the variation function is the product of a set of one-electron functions g_i and the functions g_i are varied in order to minimize the variational integral. This is an iterative process and continues until there is no further reduction in the value of the variational integral. The process involves guessing a product wavefunction, then focusing on one electron at a time, and determining the average potential acting on that one electron as a result of the charge distribution of the other electrons. For electron 1, a one-electron Schrödinger equation is solved and a better orbital is obtained. This kind of calculation is then performed on electron 2 using the better orbital for electron 1 and the orbitals of the other electrons besides 1 and 2 come from the initial guess for the product wave function. Once the better orbital for electron 2 is obtained, the calculation is applied to electron 3 using the better orbitals for electrons 1 and 2 and the original guessed orbitals for electrons $4, \ldots, n$. This procedure is applied eventually to all n electrons and then the cycle is repeated until the orbitals do not change any more. [6] In VSCF, the vibrational wavefunction is approximated as a product of single-mode wavefunctions, called modals. [7] The energies, effective potentials, and wavefunctions for each mode are obtained self-consistently. [7]

In this project, VSCF was applied to formaldehyde, which is the most simple carbonyl compound (Figure 2.2). Formaldehyde was chosen for study because, only having four atoms, it is simple enough that the calculations can be performed within a reasonable period of time, but it is complex enough that it has interesting vibrational motions and shows anharmonic coupling between modes. Thus it can be used effectively to test the VSCF method for determining frequencies and for use in calculating NMR parameters. There are two types of anharmonicity present in the molecular vibrations of formaldehyde and other polyatomic molecules having more than two or three atoms. One is bond dissociation anharmonicity, where the atoms dissociate as the bond length becomes very large. Another is anharmonic coupling, which is energy exchange between the different normal modes. Anharmonic coupling involves one bond increasing in length, for example the C - O bond, causing the C - H bonds to get shorter in order to preserve the electron density around the carbon atom. As the C - O bond increases in length, it becomes closer to being a single bond. Anharmonic coupling results in the normal modes of vibration not being completely independent of one another as the normal mode approximation states that they are. For example in this case the C-H symmetric stretch mode is coupled with the C-O stretch mode.

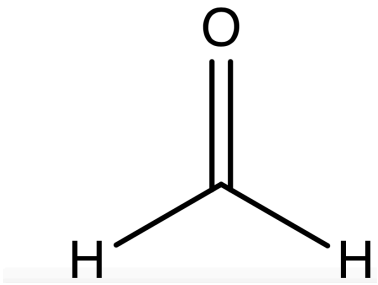

Figure 2.2: Formaldehyde.

Vibrational SCF was used to investigate amino acid dimers with protons attached to them in a study by Gerber *et al*. [5] Specifically, correlation-corrected VSCF was used to calculate the anharmonic frequencies of vibration of two amino acid dimers with protons attached: $GlyLysH^+$ and $GlyGlyH^+$ (Figures 2.3 and 2.4). The VSCF anharmonic frequencies were closer to experimental values than the harmonic frequencies for most of

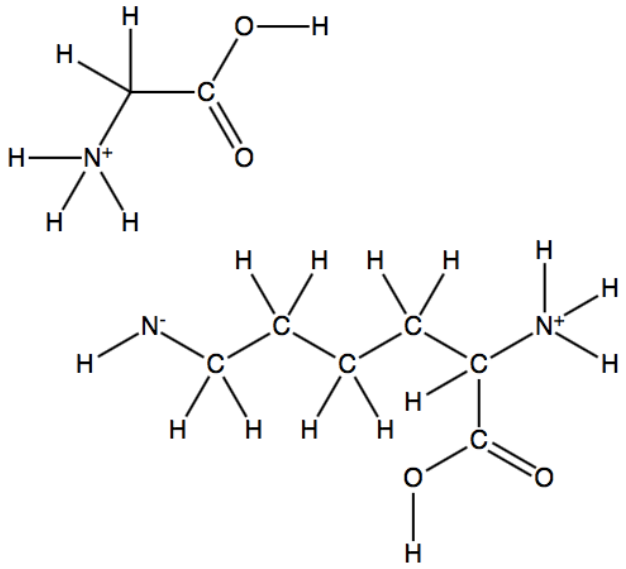

Figure 2.3: $GlyLysH^+$

the modes of vibration of $GlyLysH^+$ and for all of the modes of vibration of $GlyGlyH^+$.

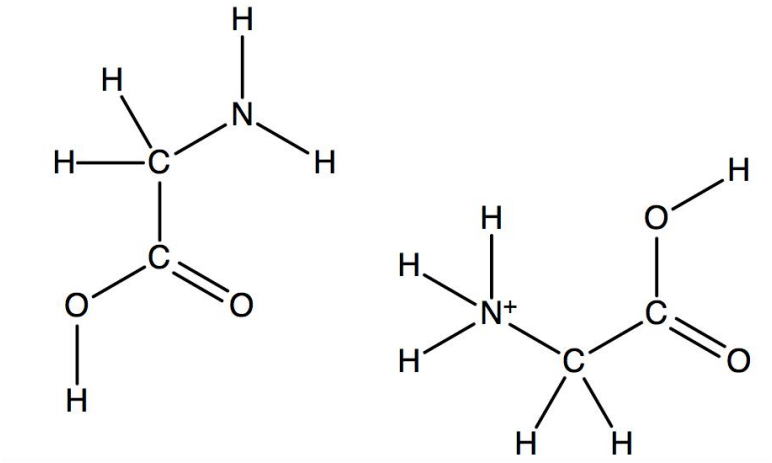

Figure 2.4: GlyGlyH+

Vibrational SCF was used according to a paper by Gerber *et al*. [8] to investigate the anharmonic frequencies of the mutant DNA base 5,6-dihydrouracil, shown in Figure 2.5, and also those of the complex of 5,6-dihydrouracil with water, shown in Figure 2.6. The emphasis was on determining the anharmonic coupling between the normal modes of vibration. 5,6-dihydrouracil is formed by oxidation of cytosine, a phenomenon that can lead to cancer. The CO out-of-plane bending mode coupled anharmonically with the NH stretch mode at 3478 cm^{-1} in 5,6-dihydrouracil.

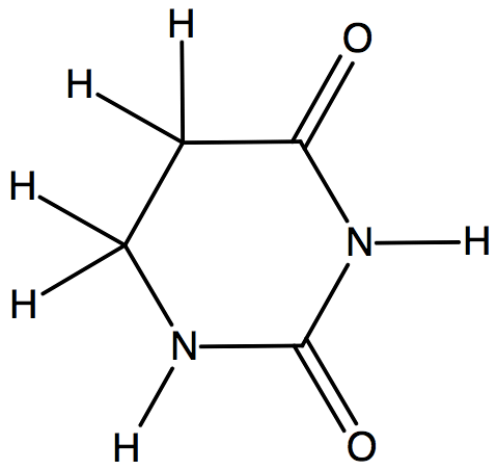

Figure 2.5: 5,6-dihydrouracil

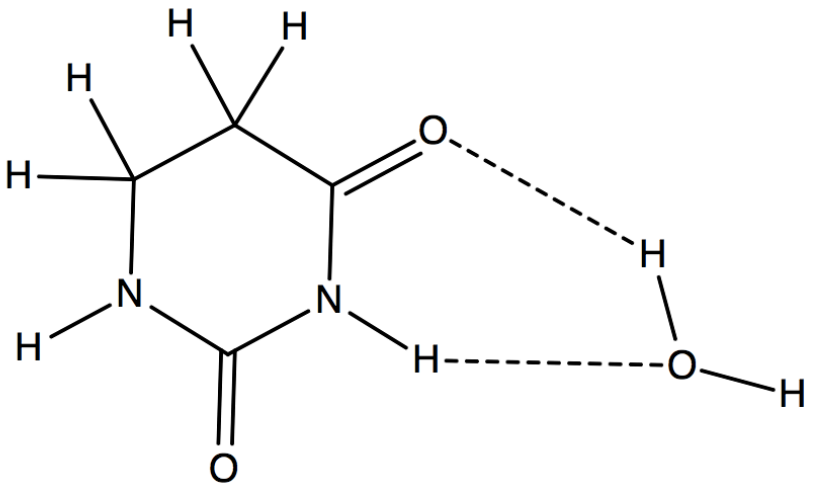

Figure 2.6: 5,6-dihydrouracil-water complex.

According to a paper by Fujisaki *et al.*, vibrational SCF and vibrational configuration interaction (VCI), which is based on VSCF, were used to compute the vibrational energy relaxation pathways of *N*-methyl acetamide, the structure of which is

shown in Figure 2.7. *N*-methyl acetamide has 24 degrees of vibrational freedom.[9] The VCI wavefunction uses as a basis VSCF configurations.

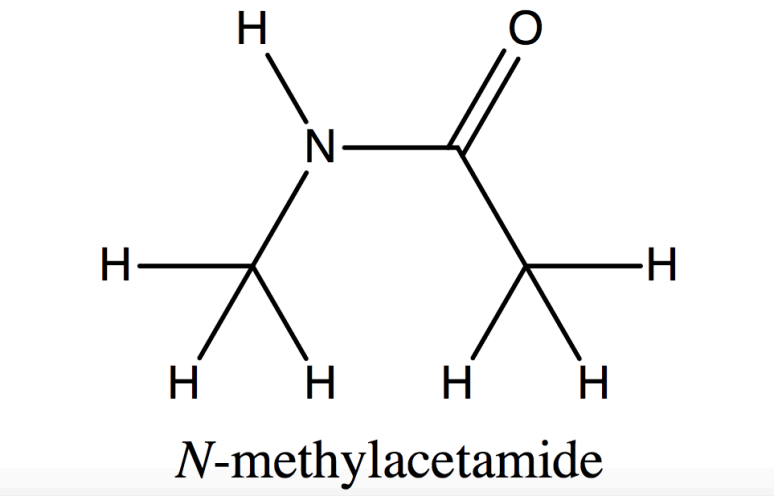

Figure 2.7: N-Methyl Acetamide.

Vibrational SCF was used to analyze anharmonic vibrations of bovine pancreatic trypsin inhibitor (BPTI) protein as reported in *Science* 1995. [10] Among other things, the Debye-Waller factors were calculated for the protein. Debye-Waller factors are measures of the mean-square fluctuation of interatomic distances in a crystal.[11starstar] In a crystal of a mixture of two elements, if one element has a higher Debye-Waller factor, it will have a larger amplitude of vibration with temperature being held constant throughout the crystal. A fourth-order Hamiltonian was used to account for anharmonicities. This was not quantum chemistry but involved molecular mechanics or classical mechanics because the size of a protein is too large to apply quantum chemical calculations.

A VSCF study along with Raman spectroscopic analysis was done on photoactive yellow protein (PYP) according to a paper by Adesokan *et al.* [12] The dark state of the protein and also two intermediate forms of the protein that form as a result of photoactivation were investigated. Simpler small molecule models were used for the three forms of the protein. For the dark form of the protein, unprotonated cis-4-hydroxy-cinnamyl methyl thiolester was used together with methanol to mimic Tyr42, acetic acid to mimic Glu46, and methylamine to mimic Cys69 (Figure 2.8).

For the blueshifted PYP_M form of the protein, protonated cis-4-hydroxy cinnamyl methyl thiolester was used with methylamine to mimic Cys69 (Figure 2.9). For the redshifted PYP_L form of the protein, cis-4-hydroxy cinnamyl methyl thiolester was used with methanol to mimic Tyr42 and acetic acid to mimic Glu46 (Figure 2.10). Frequencies of vibration determined from the calculation corresponded well with frequencies determined by Raman spectroscopy for the actual protein.

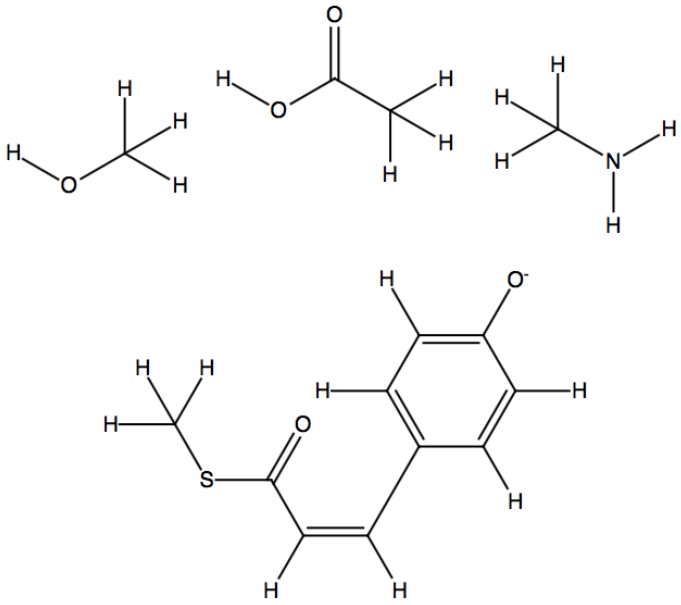

Figure 2.8: Model of PYP consisting of cis-4-hydroxy-cinnamyl methyl thiolester with methanol to mimic Tyr42, acetic acid to mimic Glu46, and methylamine to mimic Cys69.

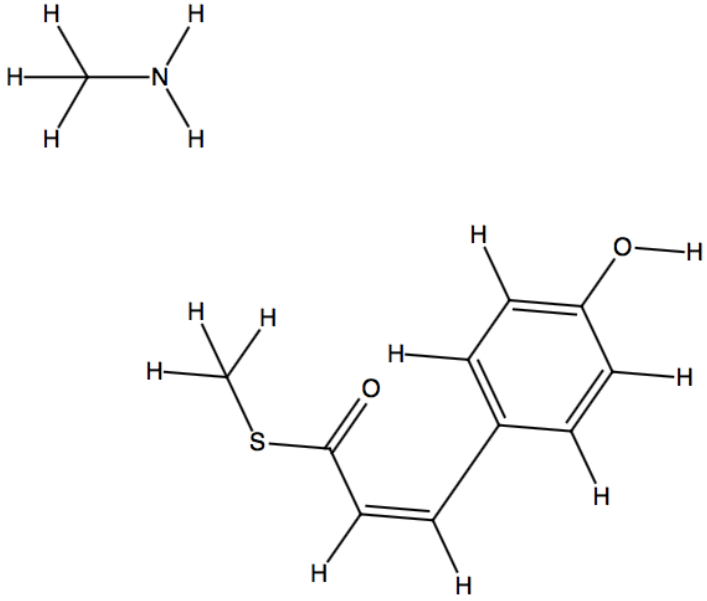

Figure 2.9: Model of PYP consisting of protonated cis-4-hydroxy-cinnamyl methyl thiolester with methylamine to mimic Cys69.

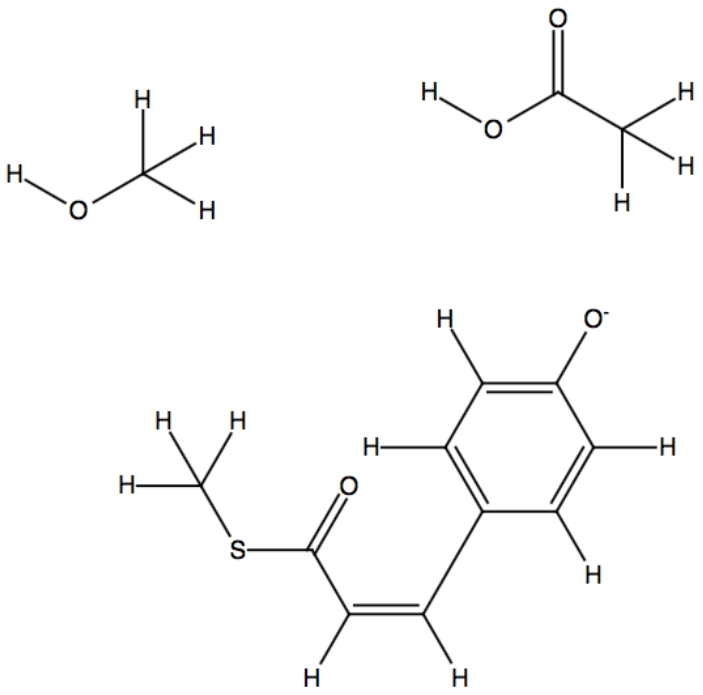

Figure 2.10: Model of PYP consisting of cis-4-hydroxy-cinnamyl methyl thiolester with methanol to mimic Tyr42 and acetic acid to mimic Glu46.

Formaldehyde possesses C_{2v} symmetry. It has a single two-fold axis of rotational symmetry that passes through the carbon and the oxygen. If the molecule is rotated 180 degrees about the axis of symmetry, it will have a configuration indistinguishable from its original configuration. Thus it has two equivalent, indistinguishable configurations, and this is the meaning of the number "2" in "C_2v". It also has two mirror planes in which the two-fold rotational axis falls. The labeling of these two planes is arbitrary.

Formaldehyde has 6 normal modes of vibration. The normal modes, their frequencies, and whether or not they preserve the C_2v symmetry of the molecule are summarized in Table 1. Normal modes of vibration that preserve the symmetry of a molecule are called fully symmetric modes; normal modes that do not preserve the symmetry of a molecule are not fully symmetric.

In a paper by Seidler *et al.* from 2007, it was reported that infrared intensities and Raman activities were calculated for formaldehyde using anharmonic wave functions. [14] Both VSCF and VCI were used for this purpose. The calculated infrared activities and Raman activities corresponded well with experimental values.

Table 2.1: Normal modes of vibration of formaldehyde and their experimental frequencies. [13]

Mode#/representation	Mode	Frequency, cm^{-1}	Fully Symmetric?
$1/1a_1$	C - H symmetric stretching	2782.5	Yes
$2/2a_1$	C - O symmetric stretching	1746.1	Yes
$3/3a_1$	H - C - H in-plane scissoring	1500.1	Yes
$4/1b_2$	C - H asymmetric stretching	2843.1	No
$5/2b_2$	H - C - H in-plane rocking	1249.1	No
$6/1b_1$	out-of-plane wagging	1167.3	No

Nuclear Magnetic Resonance (NMR) involves nuclear spins in an applied magnetic field which increases the energy difference between different spin states, and also involves a radiofrequency pulse that transfers energy to nuclear spins that are precessing at the same frequency as the pulse. [1,2] For a nucleus that has two spin states, the applied magnetic field results in one of the two spin states being slightly favored over the other due to one spin state being lower in energy than the other spin state. The spin state that is lower in energy is favored.

Spin angular momentum is a type of angular momentum that is an intrinsic property of many nuclei, and spin has a quantum number. The quantum number is denoted I. For example, a ^{1}H nucleus has a spin quantum number of $I = 1/2$. The magnitude of the spin angular momentum is proportional to I. The component of spin angular momentum along the z-axis is directly proportional to m_I, where $m_I = I, I - 1, \dots, -I$. A nucleus with spin $I = 1/2$, such as ^{1}H, has two states, α associated with $m_I = +1/2$ and β associated with $m_I = -1/2$. For ^{1}H, the β state is higher in energy

than the α state. Nuclei with spins $I > 0$ also have a magnetic moment that has direction

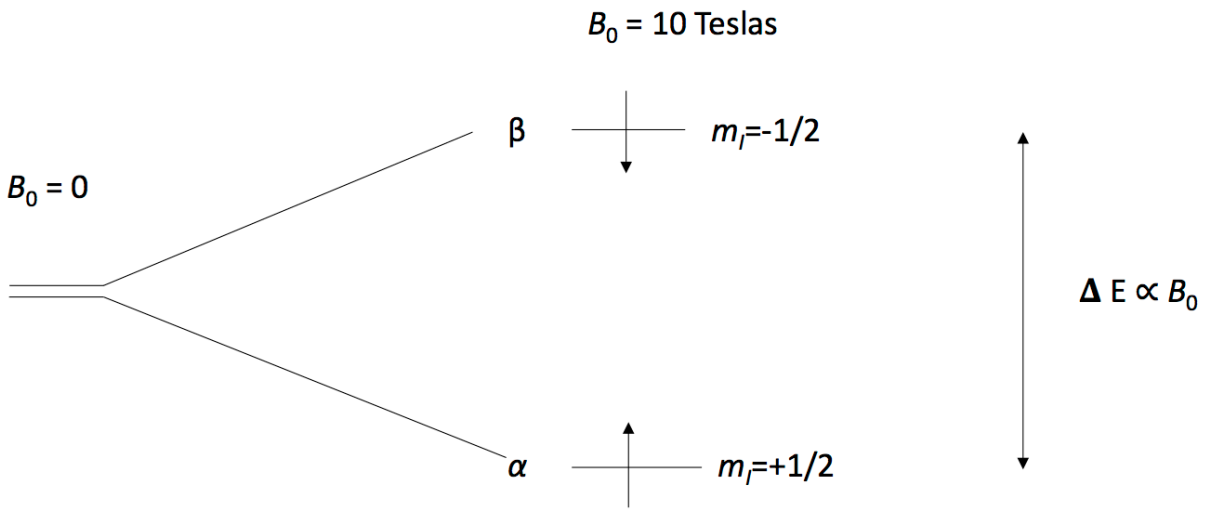

Figure 2.11: Nuclear spins energy diagram for *I* = 1/2.

based on m_I.

When a magnetic field is applied to the ^{1}H atom in an NMR spectrometer, the energy separation between α and β spin states increases from what it would be in the earth's magnetic field alone. In particular, the energy separation of the α and β spin states is directly proportional to the applied magnetic field strength (Figure 2.11). [1,2]

The following equation is used to determine the population difference between α and β spin states for nuclei of an atom that has a spin quantum number $I = 1/2$:

$$N_\alpha - N_\beta \approx \frac{N\gamma\hbar B_0}{2kT}, N = N_\alpha + N_\beta \qquad (2.15)$$

This equation is calculated based on the Boltzmann distribution with the assumptions that $E_\beta - E_\alpha << kT$ and that N_α is relatively close to N_β. For free protons in a magnetic field strength of 10 Teslas, at a temperature of 293 K, only 35 more spins in a million are in the α state than are in the β state. This is not a large difference, but is enough to be observed in the NMR spectrum with a large enough sample size. The characteristic frequency of precession of a nucleus in an applied magnetic field of strength B_0 is known as the Larmor frequency of that type of atom.

For example, the Larmor frequency of ^{1}H is 427 MHz in an applied magnetic field of strength 10 Tesla. Resonance occurs when the frequency of the applied radiofrequency pulse caused by oscillating magnetic fields matches the Larmor frequency of the nucleus of an analyte. In resonance for spin-$1/2$ nuclei, the energy of the applied radiofrequency photon matches the difference in energy between the β and α states of the nucleus, so energy flow occurs between the radiofrequency pulse and the nuclear spin.

In NMR, there are direct interactions of the nuclear spins with the applied magnetic field which are included in the external spin Hamiltonian. [15] These include interactions with the static field, with the radiofrequency field, and possibly with a gradient field. There is also an internal spin Hamiltonian that includes the following interactions: indirect interactions with the applied magnetic field mediated by electrons, and both direct interactions of the nuclear spins with each other and indirect interactions of the nuclear spins with each other mediated by the electrons. Finally, there is a chemical shielding, which will be of the most interest to us; it involves the modulation of the external magnetic field by the molecular electrons. The chemical shielding has two components: the diamagnetic shielding, which is a reduction in the applied field by the induced rotation of the electrons; and the paramagnetic shielding, which is an augmentation of the applied field caused by mixing of paramagnetic excited states into the (usually) diamagnetic ground state by the applied field.

The external spin interactions are greater than the internal spin interactions in most cases. [15]

In NMR, the chemical shift is determined by comparing the analyte to a reference compound. The formula for chemical shift is:

$$\delta = \frac{\nu - \nu^0}{\nu^0} \times 10^6 \qquad (2.16)$$

ν^0 is the reference compound nucleus resonance frequency, and ν is the analyte compound nucleus resonance frequency.

Shielding occurs because the nuclei in a compound are surrounded by electronic motion from the electrons in the molecule and as a result experience a different, and generally larger, magnetic field compared to the applied magnetic field. [1,2] The difference between the magnetic field experienced by the nuclei and the applied magnetic field is called δB, and it is related to the applied magnetic field B_0 by the following equation:

$$\delta B = -\sigma B_0 \qquad (2.17)$$

where σ is the shielding constant. Different nuclei of the same element in a molecule may have different shielding constants since the electronic structure may differ in different parts of the molecule and also the surrounding magnetic nuclei may differ. Thus different nuclei of the same element in a molecule may be in different magnetic environments. Stronger shielding moves the peaks of an analyte nucleus to smaller chemical shift.

The chemical shift δ is related to the shielding constants of the analyte by the formula:

$$\delta = \frac{\sigma^0 - \sigma}{1 - \sigma^0} \times 10^6 \qquad (2.18)$$

where σ^0 is the shielding constant of the reference compound nucleus and σ is the shielding constant of the analyte nucleus.

Larger values of σ are associated with smaller values of the chemical shift δ, and smaller values of σ are associated with larger values of the chemical shift δ. The absolute value of the shielding is generally unknown, because it is impossible to measure an NMR signal from a bare nucleus. Usually what is done is to use as a reference a small molecule in the gas phase whose shielding can be computed fairly accurately.

Methods

The geometry of formaldehyde in the gas phase was optimized at the MP2 level on GAMESS using each of the basis sets aug-cc-pVDZ, aug-cc-pVTZ, and aug-cc-pVQZ, and the vibrational frequencies were calculated at the MP2 level using all three basis sets.[16, 17] Then VSCF was run on formaldehyde in the gas phase using GAMESS with each of the basis sets aug-cc-pVnZ, $n = 2 - 4$. In other words, the basis sets aug-cc-pVDZ, aug-cc-pVTZ, and aug-cc-pVQZ were used. aug-cc-pVDZ is *augmented correlation-consistent polarized valence double zeta,* aug-cc-pVTZ is *augmented correlation-consistent polarized valence triple zeta,* and aug-cc-pVQZ is *augmented correlation-consistent polarized valence quadruple zeta.* The augmented-cc-pVnZ basis sets have additional diffuse functions compared to the regular Dunning cc-pVnZ basis sets. Diffuse functions are useful for modeling electrons that are spread out from the main electron density, such as for example occurs in the valence orbitals of anions. The phrase *double zeta* indicates that the basis set has two functions per atomic orbital. Similarly, *triple zeta* indicates that the basis set has three functions per atomic orbital.[18] Valence-multiple zeta basis functions are a form of split-valence basis functions which were developed based on the recognition that the valence orbitals of atoms involved in chemical bonding vary more widely than the core orbitals, and so the valence orbitals are split into multiple different functions, while only one basis function is used to model core orbitals. [14] The term "polarized valence" refers to adding a Gaussian-type orbital basis function of one quantum number higher of angular momentum than the valence orbital of the atom in question. For hydrogen this would involve adding a 'p' Gaussian-type orbital, which would then polarize the 's' functions of hydrogen.

The VSCF data file includes the wavefunctions of the ground vibrational states of each normal mode of vibration at sixteen different displacements from equilibrium. These displacements are referred to as grid points. The VSCF data file also includes, for each of the 6 normal modes of vibration, the coordinates of the molecule at each of these sixteen different displacements from equilibrium. These sets of coordinates were used to run NMR calculations on GAUSSIAN-09 to determine the chemical shieldings of each atom of the formaldehyde molecule at each grid point for each of the normal modes. Then the NMR chemical shieldings were used together with the wavefunctions to calculate the average NMR chemical shielding for each atom for each mode. The

isotropic, gauge-invariant chemical shielding values were the ones used for the calculation of the average.

The formula used to determine the average chemical shielding value is as follows:

$$\overline{\sigma} = \frac{\int_{-\infty}^{\infty} \psi^*(x)\sigma(x)\psi(x)dx}{\int_{-\infty}^{\infty} \psi^*(x)\psi(x)dx} \qquad (2.19)$$

In this case all the wavefunctions are real-valued functions, so it is true that:

$$\overline{\sigma} = \frac{\int_{-\infty}^{\infty} \psi^2(x)\sigma(x)dx}{\int_{-\infty}^{\infty} \psi^2(x)dx} \qquad (2.20)$$

The wavefunctions also happen to be positive at all displacements from equilibrium.

Two methods were used to compute the average chemical shielding value. One was a numerical integration method using a Microsoft Excel spreadsheet, and the other involved fitting the wavefunctions to Hermite polynomials and the chemical shielding values to regular polynomials $a + bx + cx^2 + \cdots$, and then using analytical integration to calculate the areas under the curves. The software Mathematica was used for fitting the data to polynomials and analytical integration. The average chemical shielding was computed at two levels of theory, Hartree-Fock and MP2. MP2 involves second-order many-body perturbation theory. MP2 adds to the Hartree-Fock energy a correction term to account for electron-electron repulsion. An additional NMR calculation was run at the equilibrium conformation of the molecule. Then the NMR chemical shieldings for each mode were compared with the equilibrium NMR chemical shielding values and the sum of the differences from equilibrium was taken across all six modes.

The two hydrocarbons methane and ethylene were also analyzed by VSCF for their normal modes of vibration, and NMR chemical shielding constants were computed from the coordinates at each of the grid points which represent displacements along the normal modes.

Results

The frequencies calculated from different basis sets were compared to determine whether convergence occurs as the basis set size increases. Figure 2.12 shows the normal modes of formaldehyde; mode numbers have been assigned based on the conventions formulated by Herzberg [19]. The frequencies calculated for formaldehyde using each of the three basis sets are plotted alongside each other for each of the six normal modes in Figures 2.15-2.18. It appears that the frequencies converge to some extent. The calculated frequencies at the anharmonic VSCF-PT2 and harmonic levels are reported alongside experimental values for each mode in Tables 2.2-2.4. ΔE_{diag} and ΔE_{coup} are also reported in these tables. ΔE_{diag} measures the extent to which the bond dissociation

anharmonicity affects the frequency of a mode and ΔE_{coup} is a measure of how much anharmonic coupling affects the frequency of a mode. [5] Based on the values of ΔE_{coup}, the asymmetric stretch mode (mode $1b_2$) has the greatest amount of anharmonic coupling while the C-O stretch mode (mode $2a_1$) has the least amount of anharmonic coupling. Based on the values of ΔE_{diag}, the asymmetric stretch mode has the greatest amount of bond dissociation anharmonicity while the H-C-H in-plane scissoring mode (mode $3a_1$) has the least amount of bond dissociation anharmonicity.

Figures 2.16-2.20 summarize the frequencies calculated for each mode of formaldehyde and their differences from experimental values. As shown in Figure 2.15, the VSCF-PT2 calculated frequencies consistently approach experimental values for modes $2a_1$, $2b_2$, and b_1 as the basis set size increases from $\zeta = 2$ to $\zeta = 3$ to $\zeta = 4$. For modes $1b_2$ and $1a_1$, the smallest basis set predicts frequencies closest to experimental values. For mode $3a_1$ the middle sized basis set predicts the frequency most accurately.

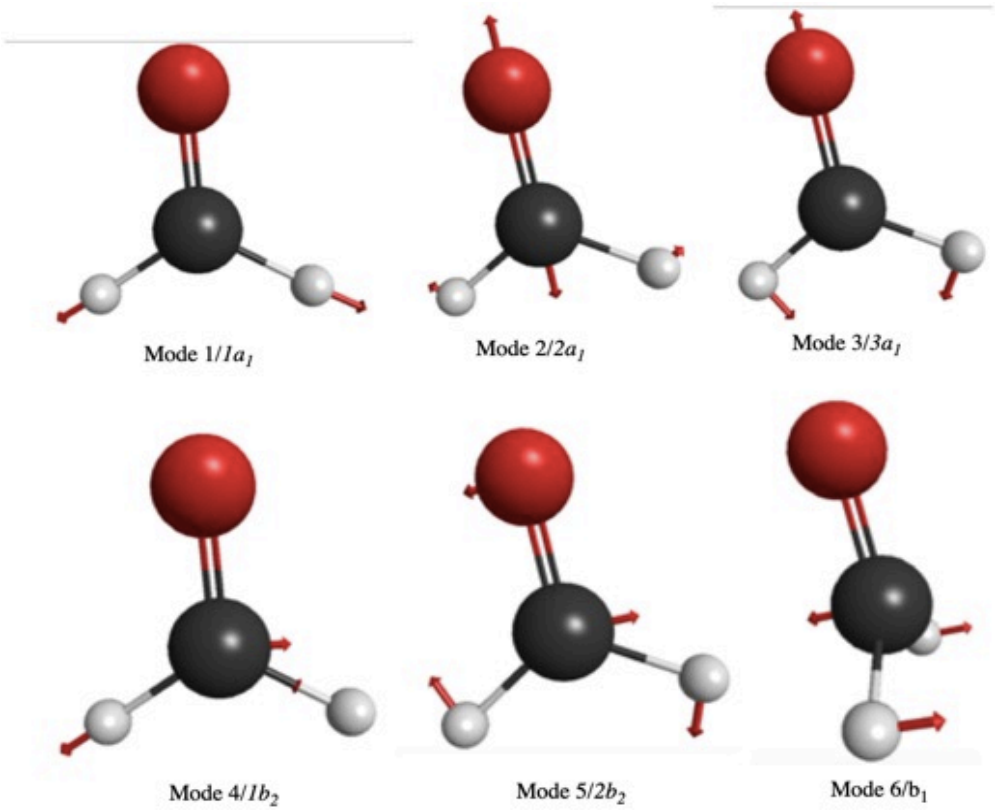

Figure 2.12. Formaldehyde normal modes of vibration; numbering according to Herzberg [19].

Figures 2.17-2.20 show the deviations or differences from the experimental values for both harmonic and anharmonic VSCF-PT2 frequencies, and the anharmonic frequencies are closer to experiment in most cases. As seen in Figure 2.17, there is almost no deviation from experiment for the $\zeta = 2$ anharmonic frequency for the C-H asymmetric stretching mode (mode $1b_2$).

Table 2.2: Formaldehyde aug-cc-pVDZ frequencies, cm^{-1}, compared with experiment and ΔE values. ΔE values are given in cm^{-1}.

Mode #/Representation	Diagonal Freq.	Exp. Freq.	aug-cc-pVDZ VSCF-PT2 Freq.	aug-cc-pVDZ Harmonic Freq.	$\lvert\Delta E\rvert_{diag}$	$\lvert\Delta E\rvert_{coup}$
$1/1a_1$	2915.07	2782.5	2815.17	2977.59	62.52	99.9
$2/2a_1$	1711.65	1746.1	1695.60	1726.75	15.1	16.05
$3/3a_1$	1527.33	1500.1	1490.67	1526.91	0.42	36.66
$4/1b_2$	3133.36	2843.1	2843.17	3061.72	71.64	290.19
$5/2b_2$	1263.32	1249.1	1226.67	1252.04	11.28	36.65
$6/b_1$	1203.94	1167.3	1151.09	1188.19	15.75	52.85

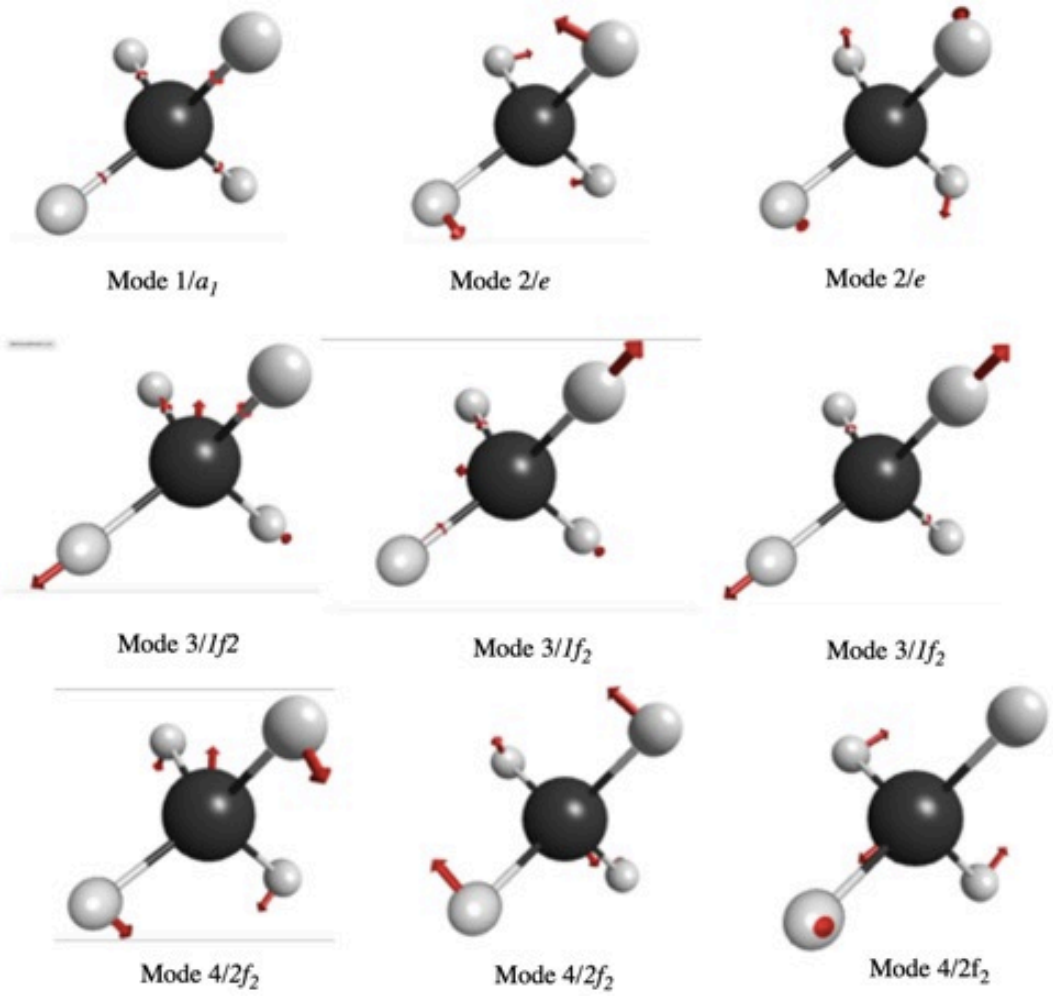

Figure 2.13. Normal modes of methane. Numbering according to Herzberg [19].

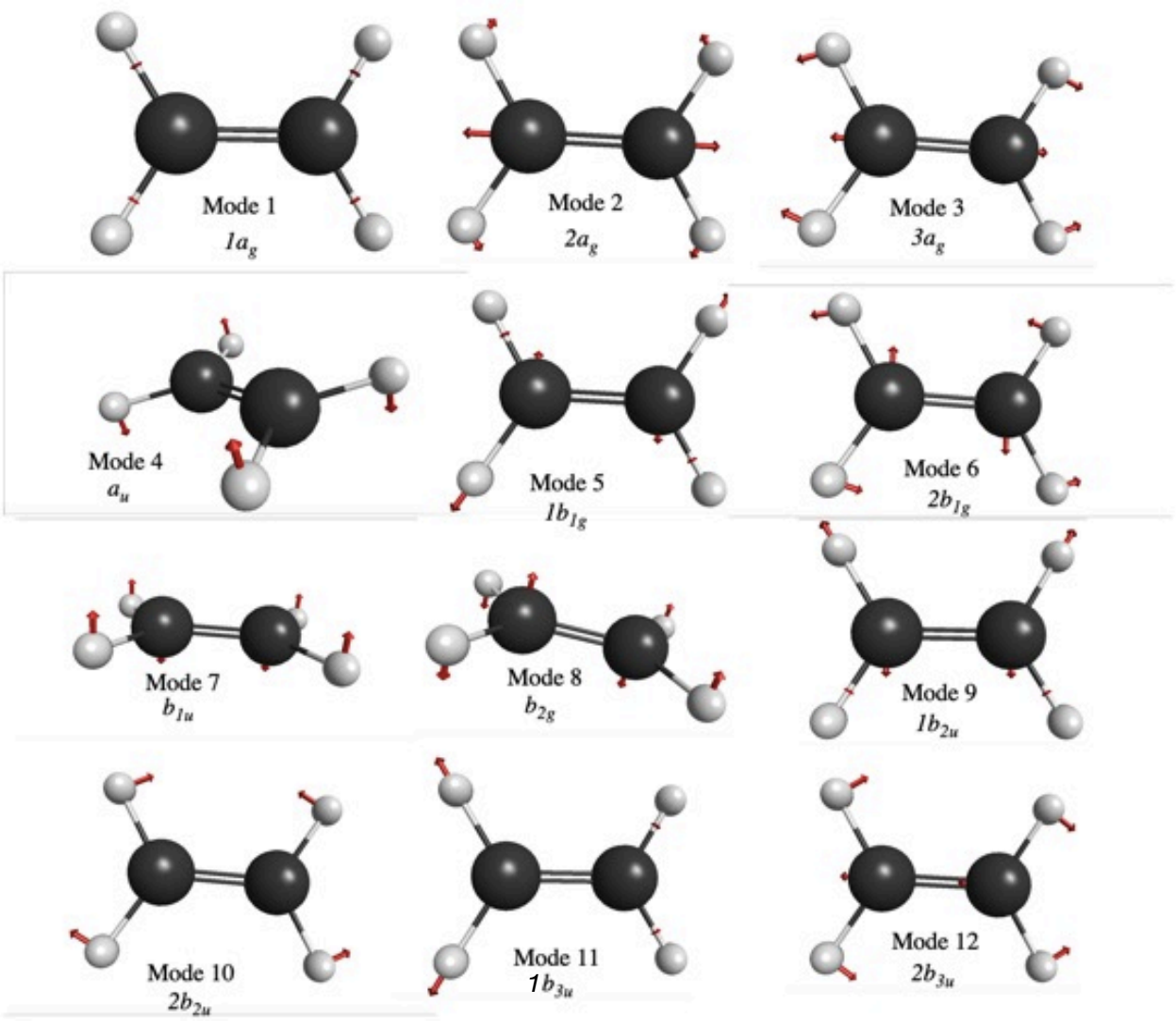

Figure 2.14. Normal modes of ethylene. Numbering according to Herzberg.

Table 2.3: Formaldehyde aug-cc-pVTZ frequencies, cm^{-1}, compared with experiment and ΔE values. ΔE values are given in cm^{-1}.

Mode #	Diagonal Freq.	exp. Freq.	aug-cc-pVTZ VSCF-PT2 Freq.	aug-cc-pVTZ Harmonic Freq.	$\lvert\Delta E\rvert_{diag}$	$\lvert\Delta E\rvert_{coup}$
$1/1a_1$	2913.91	2782.5	2819.28	2973.39	59.48	94.63
$2/2a_1$	1736.5	1746.1	1721.28	1752.76	16.26	15.22
$3/3a_1$	1540.87	1500.1	1504.68	1540.05	0.82	36.19
$4/1b_2$	3121.09	2843.1	2837.12	3047.59	73.5	283.97
$5/2b_2$	1277.92	1249.1	1241.69	1266.85	11.06	36.23
$6/b_1$	1214.71	1167.3	1163.24	1197.06	17.65	51.47

Table 2.4: Formaldehyde aug-cc-pVQZ frequencies compared with experiment and ΔE values. Frequencies and ΔE values are given in cm^{-1}.

Mode #/Mode	Diagonal Freq.	exp. Freq.	aug-cc-pVQZ VSCF-PT2 Freq.	aug-cc-pVQZ Harmonic Freq.	$\lvert\Delta E\rvert_{diag}$	$\lvert\Delta E\rvert_{coup}$
$1/1a_1$	2914.35	2782.5	2818.90	2974.38	60.03	95.45
$2/2a_1$	1743.7	1746.1	1728.53	1760.43	16.73	15.17
$3/3a_1$	1543.79	1500.1	1506.92	1543.02	0.77	36.87
$4/1b_2$	3124.29	2843.1	2839.51	3052.08	72.21	284.78
$5/2b_2$	1282.8	1249.1	1245.86	1272.03	10.77	36.94
$6/b_1$	1217.68	1167.3	1166.01	1200.62	17.06	51.67

Table 2.5: Formaldehyde chemical shielding difference from equilibrium, ppm, with basis set aug-cc-pVDZ

Atom	Analytical HF	Numerical HF	Analytical MP2	Numerical MP2
C	-5.11	-4.69	-2.45	-2.14
O	-24.97	-23.10	-13.88	-12.61
H	-0.84	-0.63	-0.67	-0.51
H	-0.55	-0.63	-0.47	-0.51

Table 2.6: Formaldehyde chemical shielding difference from equilibrium, ppm, with basis set aug-cc-pVTZ.

Atom	Analytical HF	Numerical HF	Analytical MP2	Numerical MP2
C	-4.68	-4.65	-2.61	-5.04
O	-33.22	-23.38	-10.56	-27.29
H	-0.65	-0.65	-0.54	-0.59
H	-0.65	-0.65	-0.54	-0.59

Table 2.7: Formaldehyde chemical shielding difference from equilibrium, ppm, with basis set aug-cc-pVQZ

Atom	Analytical HF	Numerical HF	Analytical MP2	Numerical MP2
C	-4.73	-4.73	-2.73	-2.71
O	-23.62	-24.75	-14.08	-14.99
H	-0.65	-0.58	-0.54	-0.48
H	-0.65	-0.58	-0.54	-0.48

Table 2.8: Normal mode-corrected chemical shielding values for atoms of formaldehyde, ppm, with basis set aug-cc-pVDZ

Atom	Analytical HF	Numerical HF	Analytical MP2	Numerical MP2
C	-2.11	-1.69	24.21	24.52
O	-447.75	-445.88	-285.68	-284.42
H	21.21	21.41	21.21	21.37
H	21.49	21.41	21.41	21.37

Table 2.9: Normal mode-corrected chemical shielding values for atoms of formaldehyde, ppm, with basis set aug-cc-pVTZ.

Atom	Analytical HF	Numerical HF	Analytical MP2	Numerical MP2
C	-9.89	-9.86	7.65	5.22
O	-472.70	-462.85	-330.30	-347.03
H	21.79	21.79	21.52	21.47
H	21.79	21.79	21.52	21.47

Table 2.10: Normal mode-corrected chemical shielding values for formaldehyde, ppm, with basis set aug-cc-pVQZ.

Atom	Analytical HF	Numerical HF	Analytical MP2	Numerical MP2
C	-12.58	44.05	2.34	34.08
O	-469.61	-189.62	-343.26	-186.72
H	21.81	17.05	21.47	15.45
H	21.81	17.05	21.47	15.45

Table 2.11 shows the average differences from equilibrium in chemical shielding values for methane across all the modes for methane with basis set aug-cc-pVTZ. Table 2.12 shows the average differences from equilibrium in chemical shielding values for methane across all the modes for methane with basis set aug-cc-pVDZ. There is better agreement between the two integration methods at the higher basis set level than at the lower basis set level.

Table 2.11: Methane chemical shielding differences from equilibrium, ppm, with basis set aug-cc-pVTZ.

	$\Delta\sigma_{iso}$, ppm	$\Delta\sigma_{iso}$, ppm	$\Delta\sigma_{iso}$, ppm	$\Delta\sigma_{iso}$, ppm
Atom	MP2, numerical	HF, numerical	MP2, analytical	HF, analytical
C	-12.72	-13.87	-12.73	-13.88
H	-2.37	-2.40	-2.37	-2.40
H	-2.36	-2.39	-2.37	-2.39
H	-2.39	-2.42	-2.39	-2.42
H	-2.39	-2.42	-2.39	-2.43

Table 2.12: Methane aug-cc-pVDZ data

	$\Delta\sigma_{iso}$, ppm	$\Delta\sigma_{iso}$, ppm	$\Delta\sigma_{iso}$, ppm	$\Delta\sigma_{iso}$, ppm
Atom	MP2, numerical	HF, numerical	MP2, analytical	HF, analytical
C	9.44	10.01	0.05	-0.29
H	1.59	1.57	-0.14	-0.17
H	1.59	1.57	-0.14	-0.17
H	1.59	1.57	-0.14	-0.17
H	1.59	1.57	-0.14	-0.17

The corrected chemical shielding values for methane at the aug-cc-pVTZ MP2 level are: for ^{13}C, 190.64 ppm, and for ^{1}H, on average, 29.03 ppm.

Table 2.13: aug-cc-pVDZ frequencies for ethylene compared with experiment and ΔE values. Frequencies and ΔE values are given in cm^{-1}.

		aug-cc-pVDZ	exp.	aug-cc-pVDZ	aug-cc-pVDZ		
Mode #	Mode Repre-sentation	Diagonal Frequency	Frequency	VSCF-PT2 Frequency	Harmonic Frequency	$\lvert\Delta E\rvert_{diag}$	$\lvert\Delta E\rvert_{coup}$
1	$1a_g$	3166.97	3026.4	3038.31	3305.67	138.7	128.66
2	$2a_g$	1664.26	1622.6	1628.37	1813.72	149.46	35.89
3	$3a_g$	1373.44	1342.2	1343.12	1466.83	93.39	30.32
4	a_u	1061.38	1025.59	1031.42	1122.97	61.59	29.96
5	$1b_{1g}$	3305.3	3102.5	3121.65	3365.06	59.76	183.65
6	$2b_{1g}$	1236.49	1236	1215.94	1329.51	93.02	20.55
7	b_{1u}	1002.62	948.77	961.79	1080.76	78.14	40.83
8	b_{2g}	972.85	932.20	934.02	1093.8	120.95	38.83
9	$1b_{2u}$	3332.21	3105.5	3149.97	3393.9	61.69	182.24
10	$2b_{2u}$	859.36	825.93	826.15	883.07	23.71	33.21
11	$1b_{3u}$	3206.53	2988.64	3042.4	3283.98	77.45	164.13
12	$2b_{3u}$	1471.12	1442.48	1437.75	1573.56	102.44	33.37

Table 2.14: Ethylene differences from equilibrium, ppm, with basis set aug-cc-pVDZ.

	$\Delta\sigma_{iso}$, ppm	$\Delta\sigma_{iso}$, ppm	$\Delta\sigma_{iso}$, ppm	$\Delta\sigma_{iso}$, ppm
Atom	MP2, numerical	HF, numerical	MP2, analytical	HF, analytical
C	-3.46	-5.72	-3.44	-5.57
C	-3.46	-5.71	-3.44	-5.57
H	-0.49	-0.68	-0.51	-0.58
H	-0.51	-0.70	-0.51	-0.58
H	-0.51	-0.70	-0.51	-0.58
H	-0.51	-0.70	-0.51	-0.58

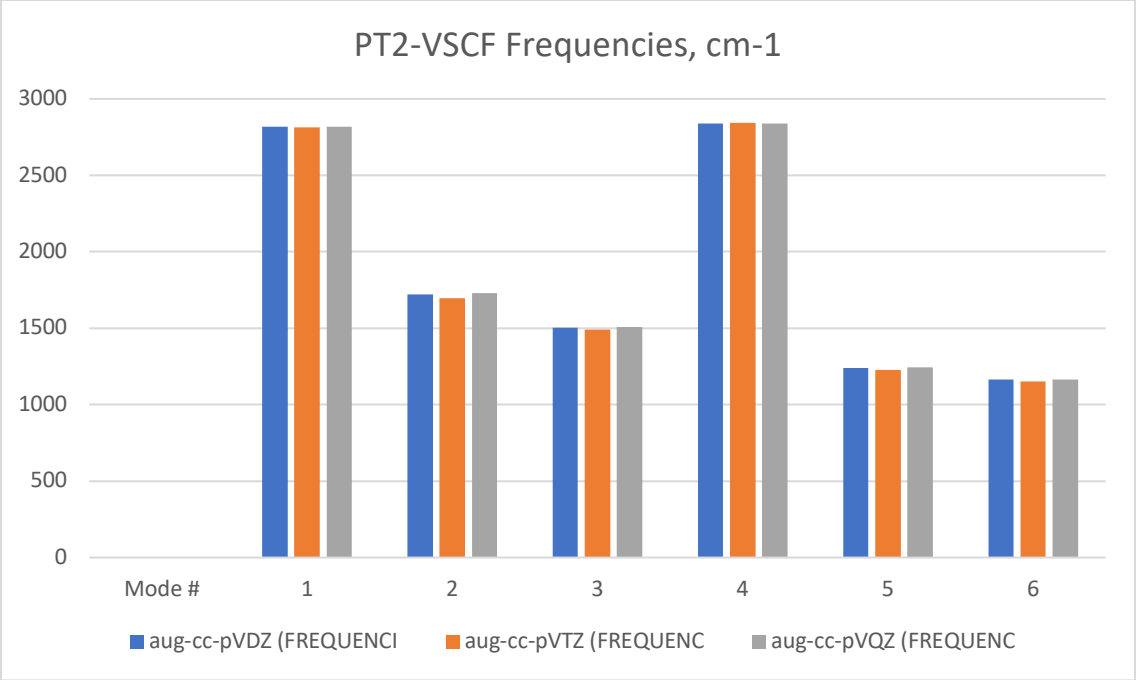

Figure 2.15. Comparison of frequencies for formaldehyde calculated with different basis sets.

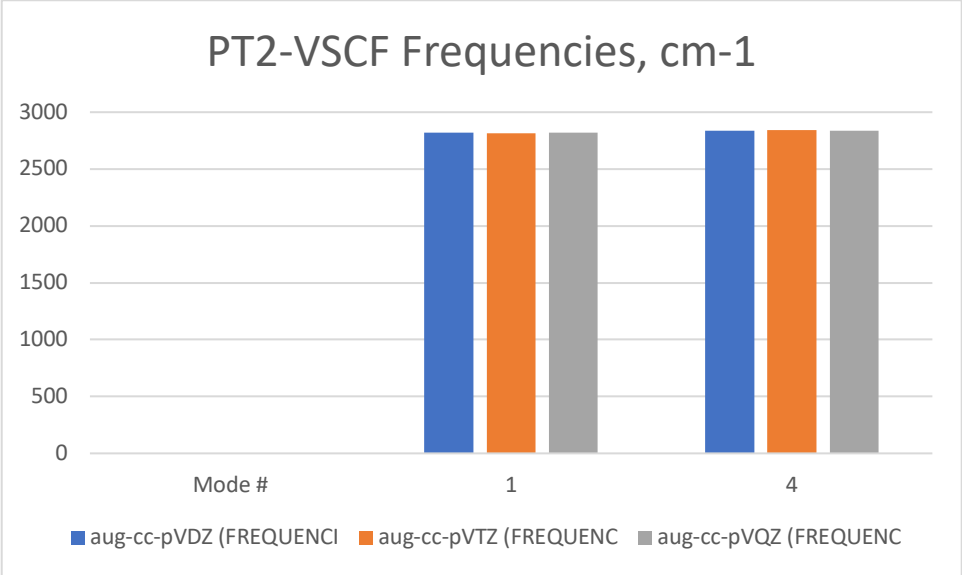

Figure 2.16: Comparing frequencies of formaldehyde calculated with different basis sets,
aug-cc-pVnZ, *n* = 2 - 4. Modes 1 and 4.

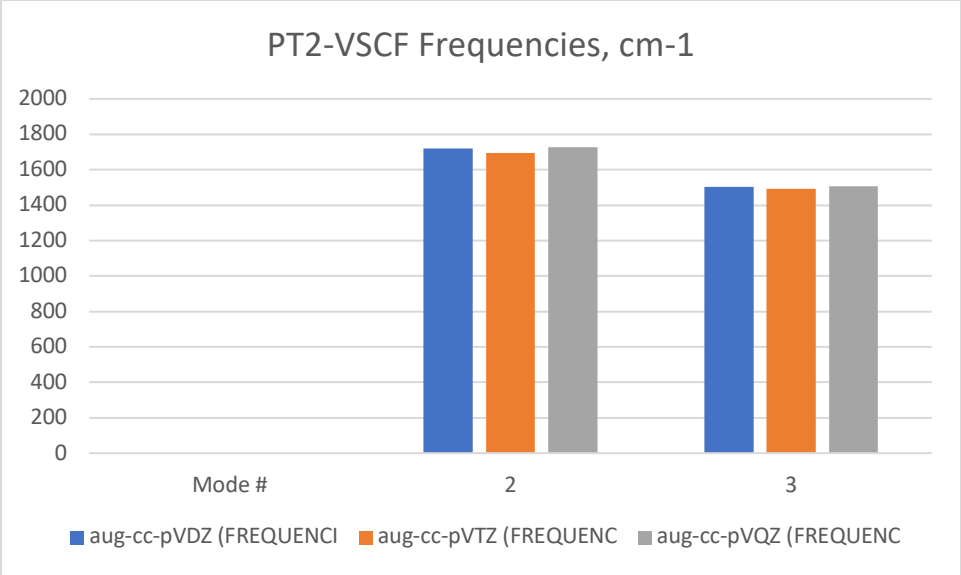

Figure 2.17: Comparing frequencies of formaldehyde calculated using different basis sets, aug-cc-pV*n*Z, *n* = 2 - 4. Modes 2 and 3.

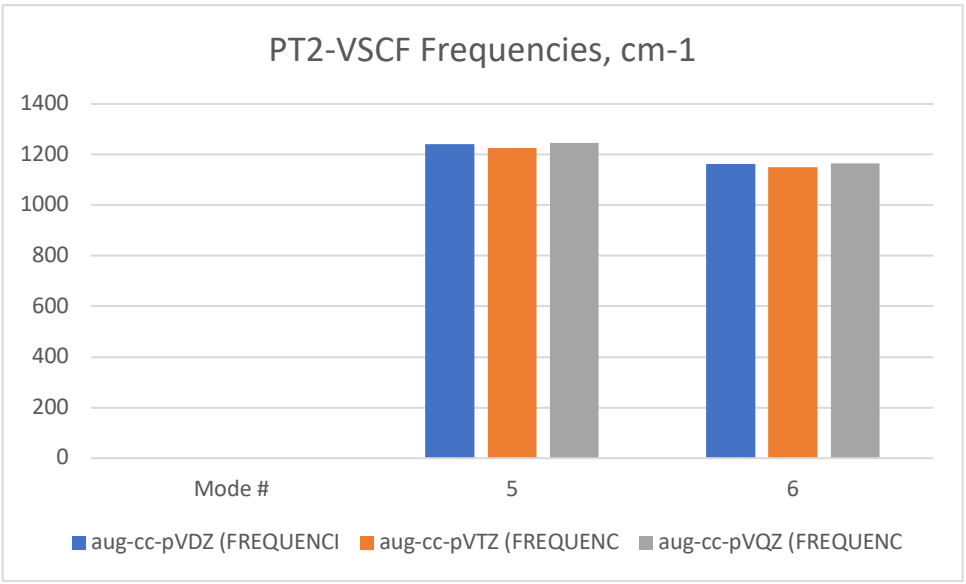

Figure 2.18: Comparing frequencies for formaldehyde calculated with different basis sets, aug-cc-pV*n*Z, *n* = 2 - 4. Modes 5 and 6.

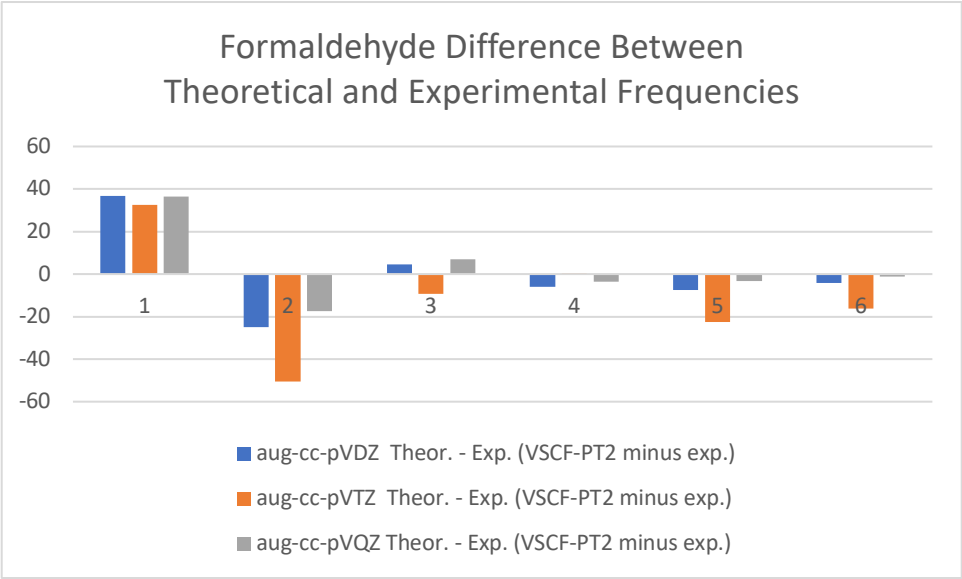

Figure 2.19. Differences between theoretical and experimental frequencies of formaldehyde normal modes for different basis sets.

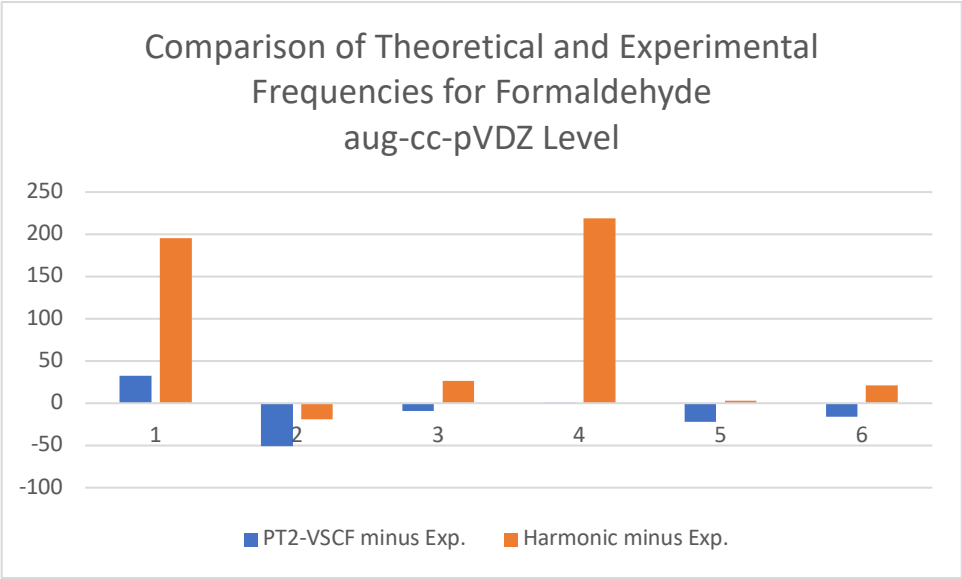

Figure 2.20: aug-cc-pVDZ differences between theoretical and experimental frequencies for formaldehyde normal modes.

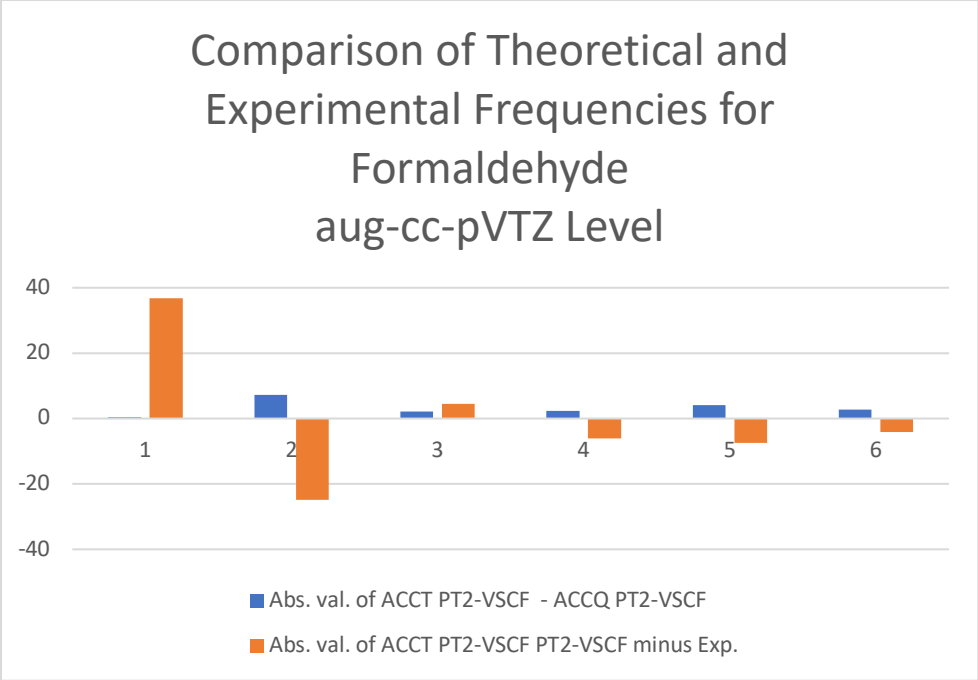

Figure 2.21: aug-cc-pVTZ differences between theoretical and experimental frequencies for formaldehyde normal modes.

The chemical shielding differences for carbon are greater than those for hydrogen which is consistent with the observation that ^{13}C NMR is more sensitive to changes in chemical

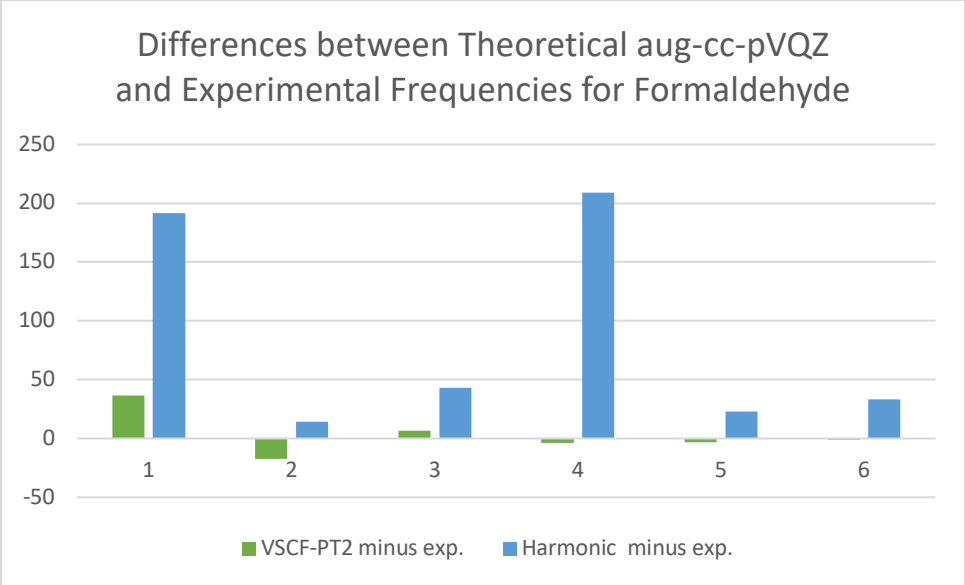

Figure 2.22: aug-cc-pVQZ Differences in Frequencies.

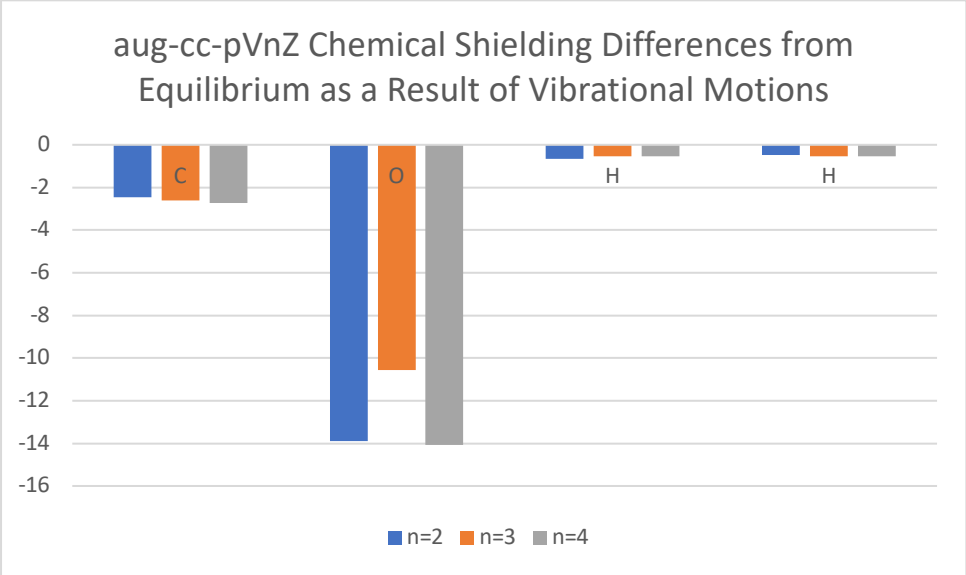

Figure 2.23: aug-cc-PV*n*Z MP2 chemical shielding differences from equilibrium for atoms of formaldehyde.

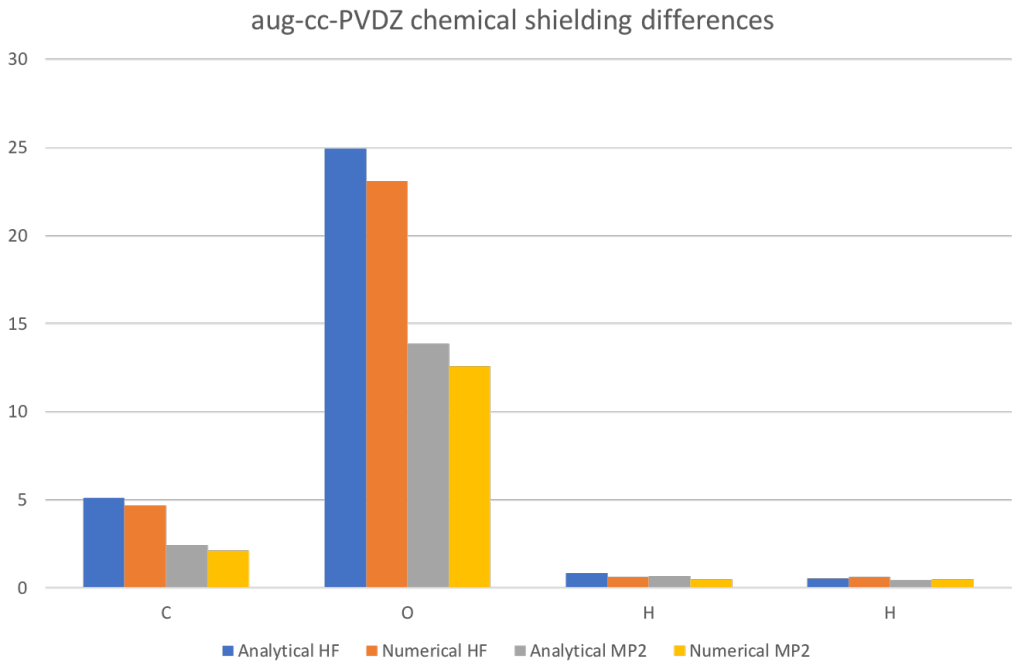

Figure 2.24. Absolute values of aug-cc-pVDZ chemical shielding differences from equilibrium for atoms of formaldehyde.

environment of the nuclei than ^{1}H NMR.

The chemical shielding differences for oxygen are the greatest out of all the atoms and this is consistent with the observation that 17-Oxygen NMR is more sensitive to changes in chemical environment of the nuclei than 13-Carbon NMR or 1-Hydrogen NMR. ^{17}O NMR chemical shifts range from about 0 to 600 ppm with H_2O standard. ^{13}C NMR shifts range from about 0 to 200 ppm with TMS standard. ^{1}H NMR shifts range from about 0 to 15 ppm with TMS standard.

For formaldehyde, the average chemical shielding differences calculated using the numerical method of integration agreed well with those calculated using the polynomial fitting and analytical integration method for the aug-cc-pVDZ basis set, but for the aug-cc-pVTZ basis set, there was more substantial deviation between values calculated by the two methods especially for oxygen. For the aug-cc-pVQZ basis set, there was not too

much deviation between values calculated by the two methods. The polynomial fitting and analytical integration method is generally more accurate than the numerical method, though the numerical method was expected to be a good approximation.

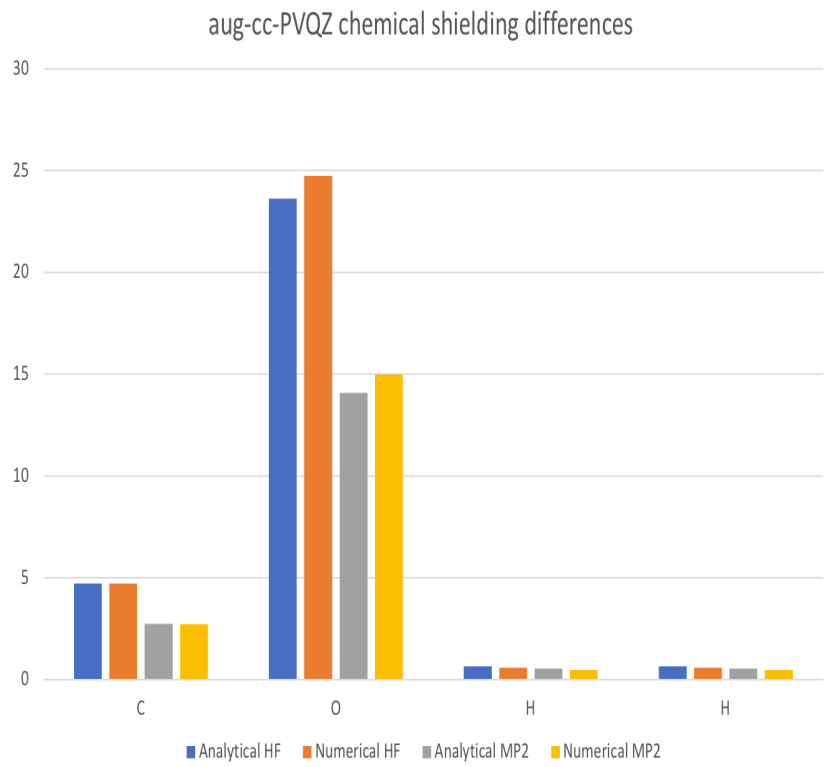

Figure 2.26: Absolute values of aug-cc-pVQZ chemical shielding differences from equilibrium for atoms of formaldehyde.

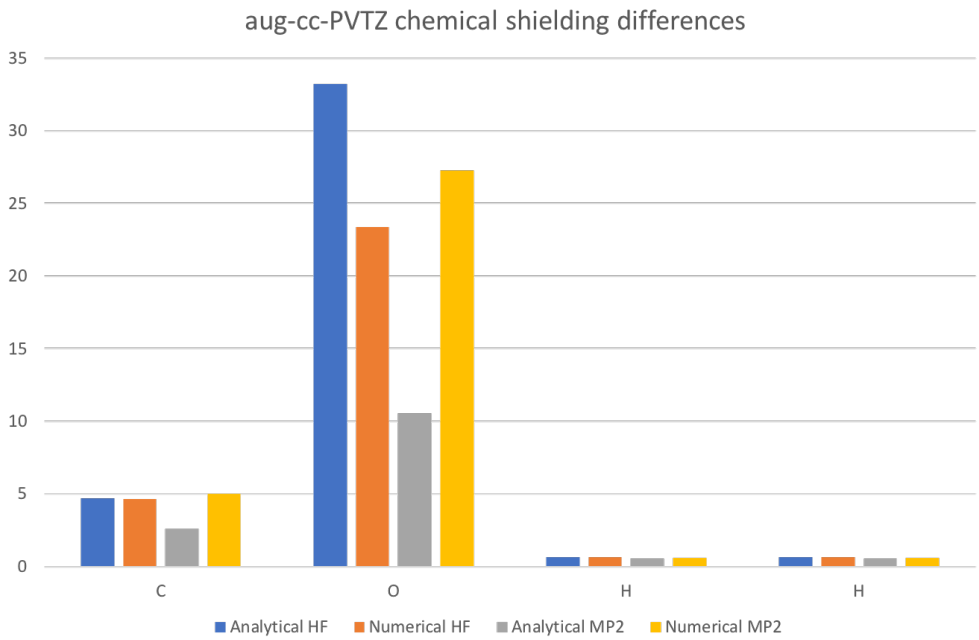

Figure 2.25: Absolute values of aug-cc-pVTZ chemical shielding differences from equilibrium for atoms of formaldehyde.

The frequencies found for the fundamental vibrations of methane in inverse centimeters from PT2-VSCF at the aug-cc-pVTZ level are as follows: 2934.16 (Mode 1/a_1), 1537.82 (Mode 2/e), 1537.70 (Mode 2/e), 3009.38 (Mode 3/$1f_2$), 3050.58 (Mode 3/$1f_2$), 3035.85 (Mode 3/$1f_2$), 1303.06 (Mode 4/$2f_2$), 1305.32 (Mode 4/$2f_2$), 1305.12 (Mode 4/$2f_2$). It can be said that there is a triply degenerate frequency at roughly 1305 cm^{-1}, that there is a doubly degenerate frequency at roughly 1538 cm^{-1}, and that there is a triply degenerate frequency around, very roughly, 3020 cm^{-1}. Figure 2.27 shows ΔE_{Diag} and ΔE_{Coup} values for methane at the aug-cc-pVTZ level. Mode 2 has the highest amount of bond dissociation anharmonicity and Mode 2 also has the least coupling anharmonicity. The most anharmonic coupling is present in Mode 3 or possibly Mode 1. Figure 2.13 shows the normal modes of methane with numbering according to Herzberg [19].

The frequencies found for the fundamental vibrations of methane in inverse centimeters from PT2-VSCF at the aug-cc-pVDZ level are as follows: 3085.24, 3085.14, 3085.22, 2934.43, 1506.21, 1506.20, 1282.83, 1282.79, 1282.80.

Ethylene was successfully calculated by VSCF MP2 using the aug-cc-pVDZ basis set. The results are as follows: the frequencies of vibration for the MP2 VSCF are, in inverse centimeters: 3038.31 (Mode 1/$1a_g$), 1628.37 (Mode 2/$2a_g$), 1343.12 (Mode 3/$3a_g$), 1031.42 (Mode 4/a_u), 3121.65 (Mode 5/$1b_{1g}$), 1215.94 (Mode 6/$2b_{1g}$), 961.79

(Mode 7/b_{1u}), 934.02 (Mode 8/b_{2g}), 3149.97 (Mode 9/$1b_{2u}$), 826.15 (Mode 10/$2b_{2u}$), 3042.4 (Mode 11/$1b_{3u}$), 1437.75 (Mode 12/$2b_{3u}$). Table 2.13 shows the values calculated for frequencies of the normal modes of ethylene. Figure 2.14 shows the normal modes of ethylene with numbering according to Herzberg [19]. Modes 1/$1a_g$, 2/$2a_g$, and 3/$3a_g$ are totally symmetric modes.

Table 2.13 shows the aug-cc-pVDZ frequencies and comparison with experiment for ethylene as well as the single-mode and coupling anharmonicity quantities for ethylene. Figure 2.28 shows the ΔE_{Diag} and ΔE_{Coup} for ethylene. Vibrational modes 1/$1a_g$, 5/$1b_{1g}$, 9/$1b_{2u}$, and 11/$1b_{3u}$ have high amounts of coupling anharmonicity. Mode 2/$2a_g$ has the highest amount of bond dissociation anharmonicity, while Mode 10/$2b_{2u}$ has the least amount of bond dissociation anharmonicity.

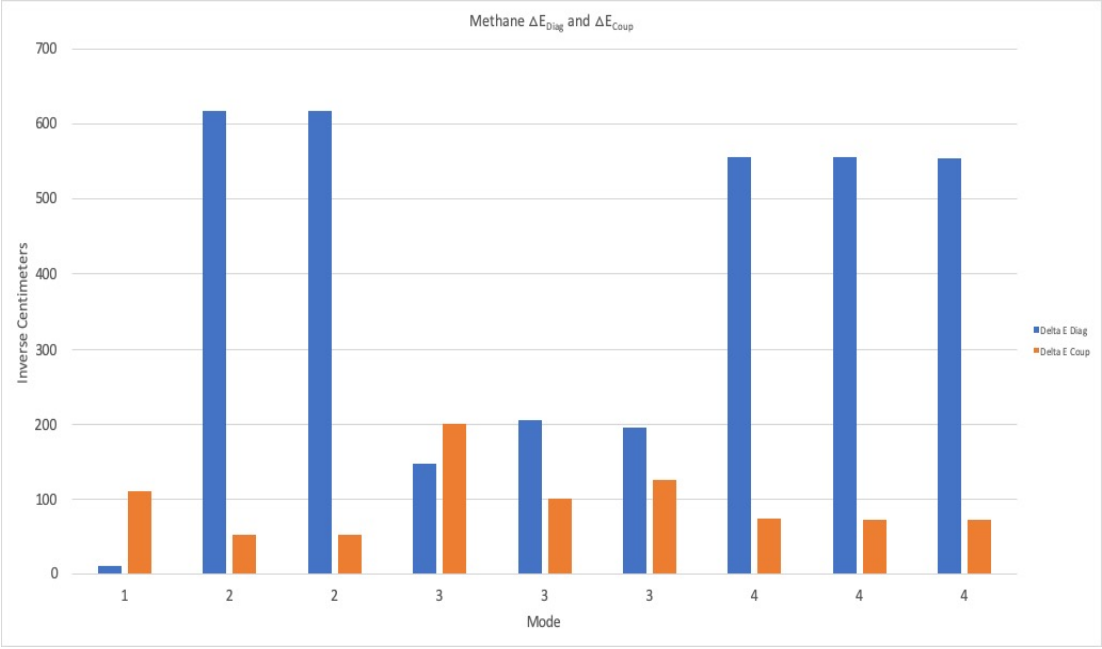

Figure 2.27. Methane Delta E_{diag} and Delta E_{Coup}.

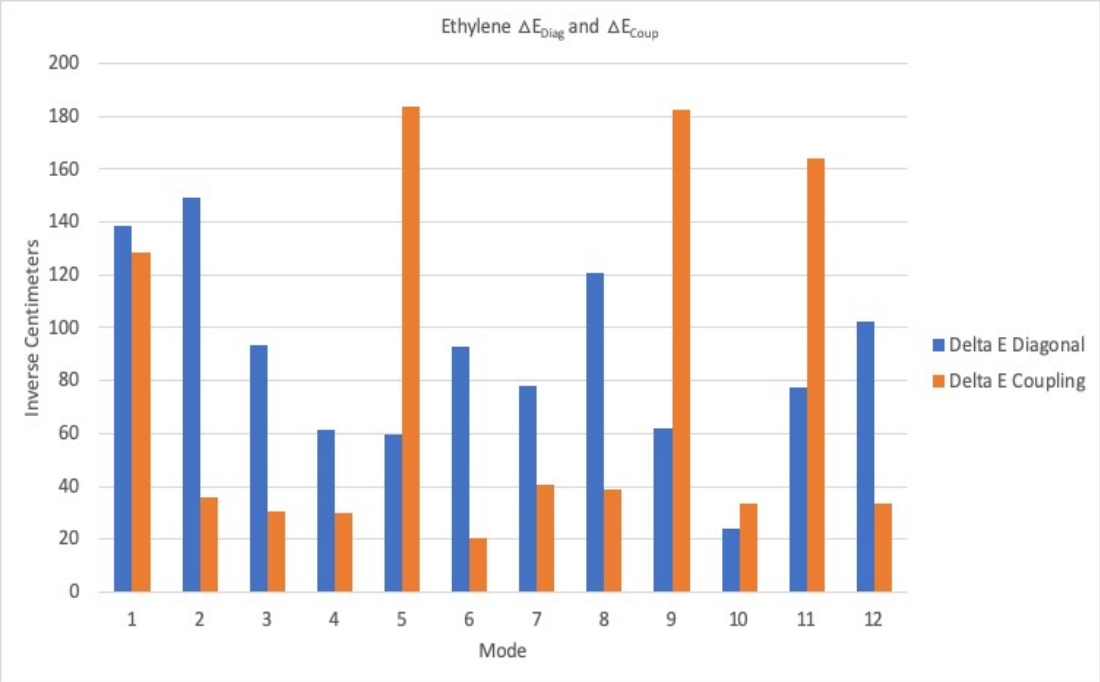

Figure 2.28: Ethylene ΔE_{Diag} and

Discussion
Basis Set Convergence

The chemical shielding differences for the atoms of formaldehyde calculated using the two methods, numerical and analytical, are shown in Tables 2.5-2.7 on page 38 for the three respective basis sets. The results are also shown graphically in Figures 2.23-2.26. Tables 2.8-2.10 on page 39 show the normal mode-corrected chemical shielding values for each atom. Table 2.15 shows experimental chemical shielding values for each atom. Figure 2.23 compares chemical shielding differences for the three ζ values for each atom. It is unclear whether there is convergence or not as basis set size increases.

In formaldehyde, mode $2a_1$ shows the greatest change in frequency as the basis set size increases. Mode $1a_1$ shows the least change in frequency as the basis set size increases.

VSCF on methane was only successfully performed with two different basis sets, so it is difficult to establish convergence. In methane, mode $1f_2$ shows the greatest change in frequency as the basis set size increases. Mode a_1 shows the least change in frequency as the basis set size increases. (labeling of modes from Herzberg, [19]).

In ethylene, the VSCF calculation was only performed with one basis set, aug-cc-pVDZ so there is nothing to compare for determining which mode is most affected by an

increase in the size of the basis set, nor can convergence be established. (numbering of modes from Herzberg[19].)

Electron Correlation

For formaldehyde the correction to HF-SCF normal mode frequencies from second-order perturbation theory was greatest for mode $1a_1$ and least for mode $2a_1$. The correction was much greater for modes $1a_1$ and $1b_2$ than for the other modes. For methane the correction to HF-SCF normal mode frequencies from second-order perturbation theory was greatest for mode a_1 and least for mode *e*. For ethylene the correction to HF-SCF normal mode frequencies from second-order perturbation theory was greatest for mode $1a_g$ and least for mode $2b_{1g}$.

Vibrational Corrections to Shielding Constants

For formaldehyde the largest vibrational correction to the carbon shielding constant comes from vibrational mode $2a_1$, which is the C—O stretching mode, and is a negative contribution. The largest vibrational correction to the oxygen shielding constant comes from mode b_1, which is a CH_2 out-of-plane wagging mode, and is a negative contribution. The largest vibrational correction to the hydrogen shielding constant comes from mode $3a_1$, which is a CH_2 scissoring mode, and is a negative contribution.

For methane the largest vibrational correction to the carbon shielding constant comes from vibrational mode $1f_2$ ($1t_2$), which is a degenerate stretching mode, and it is a negative contribution, i.e. it makes chemical shielding go downfield. The largest vibrational correction to the hydrogen shielding constant comes from mode $2f_2$ ($2t_2$), which is a degenerate deformation mode, and it is also a negative contribution.

For ethylene the largest vibrational correction to the carbon shielding constant comes from vibrational mode $2a_g$, which is a C—C stretching mode, and is a negative contribution. The largest vibrational correction to the hydrogen shielding constant comes from mode $1a_g$, which is a CH_2 symmetric stretching mode, and is a negative contribution.

Anharmonic Correction

For formaldehyde, the anharmonic correction to the frequency from the VSCF calculation is greatest in mode $1b_2$, the asymmetric C—H stretch mode, followed by mode $1a_1$, the symmetric C—H stretch mode; modes $1b_2$ and $1a_1$ have much higher amounts of anharmonic correction than the other modes. The anharmonic correction to the frequency from the VSCF calculation is least in mode b_1, the in-plane rocking mode. For methane at the aug-cc-pVTZ MP2 level, the anharmonic correction to the frequency from the VSCF calculation is greatest in mode *e* and least in mode a_1. For ethylene at the aug-cc-pVDZ MP2 level, the anharmonic correction to the frequency from the VSCF calculation is greatest in mode $1a_g$, which is a CH_2 symmetric stretch mode, mode $1b_{2u}$, which is a CH_2 asymmetric stretch mode, and mode $1b_{3u}$, which is a CH_2 symmetric stretch mode.

Comparison with Experimental Values

It has been found experimentally that the chemical shift for the oxygen in formaldehyde in liquid phase mixed with tetrahydrofuran is 656.5 ppm relative to H_2O. [20] The experimental chemical shift for the carbon in formaldehyde is either 194 ppm in THF or 196.7 ppm in dimethyl ether relative to TMS. The experimental chemical shift for the hydrogen in formaldehyde is either 9.58 ppm or 9.53 ppm relative to TMS, both values having been measured in THF by different workers. Based on these chemical shift values and the chemical shielding values of the nuclei of the reference compounds TMS and H_2O [21, 22], it was determined by using the formula $\sigma \cong \sigma^0 - \delta$ that experimental chemical shielding values are -5.9 ppm for ^{13}C, -312.5 ppm for ^{17}O, and 21.42 ppm for ^{1}H, as shown in Table 2.15. It has also been determined experimentally that the absolute chemical shielding value for ^{13}C in formaldehyde in the gas phase is -1.0 ppm.[23] This value was determined using carbon monoxide (CO) as the reference standard for measuring chemical shift. Comparing this last value with the theoretical vibrationally corrected value calculated at the aug-cc-pVQZ level, which is 2.34 ppm as calculated by the analytical integration method, the difference between the theoretical and experimental values is 3.34 ppm. Comparing the gas-phase experimental value with the numerical integration determined value at the aug-cc-pVQZ level, which is 34.08 ppm, the difference between the theoretical and experimental values is 35.08 ppm.

Table 2.15: Experimental isotropic chemical shielding values for atoms of formaldehyde.

Atom	σ_{iso}, ppm in gas phase	σ_{iso}, ppm in liquid phase
C	-1.0	-5.9
O		-312.5
H		21.42

Experimental values for methane vibrational frequencies are for ν_1 2917.0 cm^{-1}, for ν_2 1533.6 cm^{-1} (2), for ν_3 3019.5 cm^{-1} (3), and for ν_4 1306.2 cm^{-1} (3), and overtones at 2587 cm^{-1} and 3070 cm^{-1}. [24] (numbering of modes from Herzberg, [19].) Comparing the aug-cc-pVTZ/MP2 calculated frequencies with experimental values for methane normal modes: For Mode a_1 the difference between the calculated aug-cc-pVTZ MP2 frequency and the experimental value is 17.16 cm^{-1}. For Mode *e* the differences between each of the two calculated values for the frequency and the experimental value are 3.82 cm^{-1} and 3.7 cm^{-1}, respectively. For Mode $1f_2$ the differences between each of the three calculated values for the frequency and the experimental value are -10.62 cm^{-1}, 30.58 cm^{-1}, and 15.85 cm^{-1}, respectively. For Mode $2f_2$ ($2t_2$) the differences between each of the three calculated values for the frequency and the experimental value are -2.94 cm^{-1}, -0.68 cm^{-1}, and -0.88 cm^{-1}, respectively.

The experimental chemical shielding value for ^{13}C in methane in gas phase is 195.0 ppm [25]. The experimental chemical shielding for ^{1}H in methane in gas phase is

30.63 ppm [26]. Using the numerical integration method, the vibrationally corrected, at the level MP2 aug-cc-pVTZ, chemical shielding values for methane are, in ppm: 190.64 for ^{13}C and 29.03 for ^{1}H. Using the numerical integration method, the difference between the calculated at MP2 aug-cc-pVTZ and experimental ^{13}C chemical shielding values is -4.36 ppm. The difference between the The difference between the calculated, at MP2 aug-cc-pVTZ level, and experimental ^{1}H chemical shielding values is -1.60 ppm.

Using the analytical integration method, the vibrationally corrected, at the level MP2 aug-cc-pVTZ, chemical shielding values for methane are, in ppm: 190.64 for ^{13}C and 29.03 for ^{1}H. Using these values, the difference between the calculated at MP2 aug-cc-pVTZ and experimental ^{13}C chemical shielding values is -4.36 ppm, and the difference between the calculated, at MP2 aug-cc-pVTZ level, and experimental ^{1}H chemical shielding values is -1.60 ppm.

Some literature values for the fundamental vibrational frequencies of ethylene are: $\nu_1 = 3026.4\ \text{cm}^{-1}$, $\nu_2 = 1622.6\ \text{cm}^{-1}$, $\nu_3 = 1342.2\ \text{cm}^{-1}$, $\nu_4 = 1025.59\ \text{cm}^{-1}$, $\nu_5 = 3102.5\ \text{cm}^{-1}$, $\nu_6 = 1236\ \text{cm}^{-1}$, $\nu_7 = 948.77\ \text{cm}^{-1}$, $\nu_8 = 932.20\ \text{cm}^{-1}$, $\nu_9 = 3105.5\ \text{cm}^{-1}$, $\nu_{10} = 825.93\ \text{cm}^{-1}$, $\nu_{11} = 2988.64\ \text{cm}^{-1}$, $\nu_{12} = 1439.35\ \text{cm}^{-1}$. [29,30,31,32] The numbering of modes is from Herzberg [19]. These are shown in Table 2.13.

The difference between the ethylene VSCF-PT2 aug-cc-pVDZ frequencies and experimental values, in cm^{-1} is as follows: for mode $1a_g$, a C — H symmetric stretch mode, 11.91; for mode $2a_g$, the C — C stretch mode, 5.77; for mode $3a_g$, 0.92 ; for mode a_u, 5.83; for mode $1b_{1g}$, 19.15; for mode $2b_{1g}$, -20.06 ; for mode b_{1u}, 13.02; for mode b_{2g}, 1.82; for mode $1b_{2u}$, 44.47; for mode $2b_{2u}$, 0.22; for mode $1b_{3u}$, 53.76; for mode $2b_{3u}$, -4.73.

The differences from equilibrium of the chemical shielding values of ethylene are shown in Table 2.14. The corrected chemical shielding values of ethylene at the aug-cc-pVDZ MP2 level, using the numerical integration method, are 86.37 ppm for ^{13}C and 25.46 ppm for ^{1}H. The experimental chemical shielding for ^{13}C in ethylene in gas phase is 64.5 ppm [27]. The experimental chemical shielding for ^{1}H in ethylene in gas phase is 25.46 ppm [28]. The difference between calculated aug-cc-pVDZ, MP2 using the numerical method and experimental shielding for ^{13}C is 21.87 ppm. The difference between calculated MP2 aug-cc-pVDZ and experimental shielding for ^{1}H is -0.0004 ppm. The calculated aug-cc-pVDZ MP2 value for the chemical shielding of ^{13}C in ethylene using the analytical method is 86.39 ppm. The calculated aug-cc-pVDZ MP2 value for the chemical shielding of ^{1}H in ethylene using the analytical method is 25.46 ppm. The difference of the ^{13}C shielding calculated with the analytical integration method and experimental value is 21.89 ppm. The difference of the ^{1}H shielding calculated with the analytical integration method and experimental value is -0.008 ppm.

(The calculated aug-cc-pVDZ, HF chemical shielding value for ethylene for 13C, using the analytical integration method, is 66.49 ppm. The calculated aug-cc-pVDZ, HF chemical shielding value for ethylene for ^{1}H, using the analytical integration method, is 25.32 ppm. The difference between calculated aug-cc-pVDZ, HF, using the analytical integration method, and experimental shielding for ^{13}C is 1.99 ppm. The difference between calculated aug-cc-pVDZ, HF and experimental shielding for ^{1}H, using the analytical integration method, is -0.15 ppm.)

(The calculated aug-cc-pVDZ, HF chemical shielding value for ethylene for ^{13}C, using the numerical integration method, is 66.35 ppm. The calculated aug-cc-pVDZ, HF

chemical shielding value for ethylene for ^{1}H, using the numerical integration method, is 25.20 ppm. The difference between calculated aug-cc-pVDZ, HF, using the numerical integration method, and experimental shielding for ^{13}C is 1.85 ppm. The difference between calculated aug-cc-pVDZ, HF and experimental shielding for ^{1}H is -0.26 ppm.)

Conclusions

The frequencies calculated by the anharmonic VSCF-PT2 method were close to experimentally determined frequencies for the six modes of formaldehyde and there was improvement in the estimated frequencies in most cases as the basis set was expanded. In almost all cases the VSCF-PT2 calculated frequencies were closer to experimental values than the harmonic frequencies. The anharmonic coupling between modes is "nondemocratic".

For formaldehyde the largest vibrational correction to the carbon shielding constant comes from vibrational mode $2a_1$, which is the C — O stretching mode. This may result from the changing distance of the oxygen from the carbon reducing or increasing the C=O bond order. The largest vibrational correction to the hydrogen shielding constant comes from mode $3a_1$, which is a CH_2 scissoring mode. The changing distance of the hydrogen nuclei from the *pi* electrons of the carbon - oxygen double bond may reduce the chemical shielding experienced by the hydrogen nuclei i.e. protons.

In vibrational motions the contributions to chemical shielding that most obviously are changing are interactions with the valence electrons. Depending on the molecule, either all of the valence electrons are involved in bonding, as is true in methane, or some of them are in lone pairs as is the case in formaldehyde, which has two lone pairs on oxygen. The fact that for methane the largest vibrational correction to the carbon shielding constant comes from vibrational mode $1f_2$ ($1t_2$), which is a degenerate stretching mode, may mean that since in this mode, two hydrogen - carbon bond distances are decreasing at the same time as two hydrogen - carbon bond distances are increasing, having opposite trends in proximity to the 13-carbon nucleus from different pairs of protons results in a general lessening of the chemical shielding experienced by the 13-carbon nucleus. At least it can be said that having changing, both positively and negatively, hydrogen-carbon bond distances over time reduces the chemical shielding experienced by the ^{13}C nucleus. The fact that for methane the largest vibrational correction to the 1-hydrogen shielding comes from vibrational mode $2f_2$ ($2t_2$), which is a degenerate deformation mode, means that since the mode is sort of a see-saw motion, where two of the hydrogens remain in a plane with the carbon while moving up and down within the plane, one proton moving up as the other comes down, while the other two hydrogens shift back and forth from what would be a second plane perpendicular to the first plane, somehow these motions result in a lessening of chemical shielding perhaps by changing the distance of two of the protons from a carbon, thus changing the bond lengths, and also changing the distance of these two protons from each other, thus changing the distance from bonding electrons in other C - H bonds. It is thus possible that the reduction in chemical shielding experienced by the protons results from a shifting around, relative to the protons, of electron density for the valence electrons involved in bonding, though some shifting around of electron density would occur for other modes

too. (What makes this mode result in the greatest decrease in ^{1}H shielding, then, is unclear.)

The largest vibrational correction to the carbon shielding constant of ethylene comes from vibrational mode $2a_g$, which is a C — C stretching mode. This probably reflects the large paramagnetic contribution to the chemical shielding, which depends heavily on the bond-order. The largest vibrational correction to the hydrogen chemical shielding comes from mode $1a_g$, which is a CH_2 symmetric stretching mode; this mode is symmetric about two perpendicular planes, and this may mean that changing the distance of the hydrogens from the carbons affects the shielding in such a way as to decrease it. This may be due to changing carbon-hydrogen bond lengths resulting in changing orientations of the hydrogen nuclei relative to the sigma-bonding electrons of the C - H bonds. It is also possible that changing distances, both positively and negatively, of the protons from the *pi* electrons of the ethylene double bond in such a symmetrical fashion diminishes the chemical shielding experienced by the protons.

For formaldehyde, mode $1b_2$, the asymmetric C—H stretch mode, has both the greatest amount of anharmonic coupling of all the modes and has the greatest amount of anharmonic correction to the frequency of all the modes. Mode $2a_1$ has the least amount of anharmonic coupling of all the modes and while not having the least amount of anharmonic correction, it has close to the lowest amount of anharmonic correction of all the modes.

For methane, mode *e* has the highest amount of anharmonic correction to its frequency. However, mode $1f_2$ has the highest amount of coupling anharmonicity.

For ethylene, modes $1a_g$, which is a CH_2 symmetric stretch mode, $1b_{2u}$, which is a CH_2 asymmetric stretch mode, and $2b_{3u}$ have the greatest amount of anharmonic correction to their frequencies. Modes $1a_g$, $1b_{1g}$, $1b_{2u}$, and $1b_{3u}$ have the greatest amount of anharmonic coupling. So there is some overlap between the modes that have the greatest amount of anharmonic correction to their frequencies and the modes that have the most anharmonic coupling.

The agreement of the shielding constants calculated in the present study with experimental values is fairly good. For formaldehyde the difference between the calculated and experimental chemical shielding values for ^{13}C was 3.34 ppm. For methane the difference between calculated and experimental chemical shielding values for ^{13}C was -4.36 ppm. For methane the difference between calculated and experimental chemical shielding values for ^{1}H was -1.60 ppm. For ethylene the difference between the theoretical value calculated at the highest level possible with the computers available and experimental value for ^{13}C chemical shielding is 21.89 ppm, which is fairly large but not too much considering that the highest (and only) basis set at which the theoretical value was calculated was aug-cc-pVDZ. The difference between the theoretical and experimental value for ^{1}H chemical shielding for ethylene was lower, at -0.008 ppm.

References:

[1] P. Atkins, J. de Paula, Physical Chemistry, 10th Edition, New York: W. H. Freeman and Company, 2013.

[2] P. Atkins, J. de Paula, Physical Chemistry, 9th Edition, New York: W. H. Freeman and Company, 2010.

[3] D. A. McQuarrie, Statistical Mechanics, Sausalito, California: University Science Books, 2000, p. 93.

[4] E. B. Wilson Jr., J. C. Decius, P. C. Cross, Molecular Vibrations: The Theory of Infrared and Raman Vibrational Spectra, New York: Dover, 1955, pp. 15-17.

[5] A. A. Adesokan, R. B. Gerber, Anharmonic vibrational spectroscopy calculations for proton-bound amino acid dimers, J. Phys. Chem. A 113 (2009) 1905-1912.

[6] I. N. Levine, Quantum Chemistry, 7th Edition, New York: Pearson, 2014.

[7] T. K. Roy, R. B. Gerber, Vibrational self-consistent field calculations for spectroscopy of biological molecules: new algorithmic developments and applications, Phys. Chem. Chem. Phys. 15 (2013) 9468 - 9492.

[8] A. A. Adesokan, E. Fredj, E. C. Brown, R. B. Gerber, Anharmonic vibrational frequency calculations of 5,6-dihydrouracil and its complex with water: testing improved semiempirical potentials for biological molecules,
Molecular Physics 103 (2005) 1505-1520.

[9] H. Fujisaki, K. Yagi, J. E. Straub, G. Stock, Quantum and classical vibrational relaxation dynamics of
N -methylacetamide on ab initio potential energy surfaces,
International Journal of Quantum Chemistry 109 (2009) 2047-2057.

[10] A. Roitberg, R. B. Gerber, R. Elber, M. A. Ratner, Anharmonic Wave Functions of Proteins: Quantum Self-Consistent Field Calculations of BPTI, Science 268 (1995) 1319-1322.

[11starstar] E. Sevillano, H. Meuth, J. J. Rehr, Extended x-ray absorption fine structure Debye-Wailer factors. I. Monatomic crystals, Physical Review B 20 (1979) 4908 – 4911.

[12] A. A. Adesokan, D. Pan, E. Fredj, R. A. Mathies, R. B. Gerber, Anharmonic vibrational calculations modeling the Raman spectra of intermediates in the photoactive yellow protein (PYP) photocycle, J. Am. Chem. Soc. 129 (2007) 4584-4594.

[13] T. Shimanouchi, Tables of Molecular Vibrational Frequencies Consolidated Volume I, National Bureau of Standards, 1972, 1-160.

[14] P. Seidler, J. Kongsted, O. Christiansen, Calculation of vibrational infrared intensities and Raman activities using explicit anharmonic wave functions, J. Phys. Chem. A 111 (2007) 11205-11213.

[15] M. Levitt, Spin Dynamics: Basics of Nuclear Magnetic Resonance, Second Edition, Chichester, West Sussex, England, 2008.

[16] M. W. Schmidt, K. K. Baldridge, J. A. Boatz, S. T. Elbert, M. S. Gordon, J. H. Jensen, S. Koseki, N. Matsunaga, K. A. Nguyen, S. Su, T. L. Windus, M. Dupuis, J. A. Montgomery, General Atomic and Molecular Electronic Structure System, J. Comput. Chem. 14 (1993) 1347-1363.

[17double]star] M. S. Gordon, M. W. Schmidt, Advances in electronic structure theory: GAMESS a decade later, pp. 1167-1189, in "Theory and Applications of Computational Chemistry: the first forty years" C. E. Dykstra, G. Frenking, K. S. Kim, G. E. Scuseria (editors), Elsevier, Amsterdam, 2005.

[18] C. J. Cramer, Essentials of Computational Chemistry, Second Edition, Chichester, West Sussex, England: John Wiley & Sons Ltd., 2004, p. 171.

[19] G. Herzberg, Infrared and Raman Spectra of Polyatomic Molecules, New York: D. Van Nostrand Company, Inc., 1945.

[20] H. Dahn, P. Péchy, Concerning the chemical shift data ($^{17}0$, ^{13}C, 'H) of formaldehyde, Magnetic Resonance in Chemistry 34 (1996) 723-724.

[21] J. Casanovas, G. Pacchioni, F. Illas, ^{29}Si solid state NMR of hydroxyl groups in silica from first principle calculations, Materials Science and Engineering B 68 (1999) 16-21.

[22] M. Baaden, P. Granger, A. Strich, Dependence of NMR isotropic shift averages and nuclear shielding tensors on the internal rotation of the functional group X about the

C - X bond in seven simple vinylic derivatives H_2C = CH - X, Molecular Physics 98

(2000) 329- 342.

[23] Y. Wang, The Intersection of Nuclear Magnetic Resonance and Quantum Chemistry, Ph.D. Dissertation, University of Nebraska, Lincoln, NE, 2015.

[24] M. A. Thomas, H. L. Welsh, The Raman spectrum of methane, Can. J. Phys. 38 (1960) 1291 - 1303.

[25] A. A. Auer, J. Gauss, and J. F. Stanton. J. Chem. Phys. 118 (2003) 10407 – 10417.

[26] P. Garbacz, K. Jackowski, W. Makulski, and R. E. Wasylishen, J. Phys. Chem. A 2012, 116, 11896−11904.

[27] T. Zuschneid, H. Fischer, T. Handel, K. Albert, and G. Häfelinger, Z. Naturforsch. 59b (2004) 1153 – 1176.

[28] P. Garbacz, K. Jackowski, W. Makulski, and R. E. Wasylishen, J. Phys. Chem. A 116 (2012) 11896−11904.

[29] S. J. Cyvin, B. N. Cyvin, Normal coordinates and force constants of ethylene molecules, Acta Chemica Scandinavica 17 (1963) 1831 - 1842.

[30] E. Rusinek, H. Fichoux, M. Khelkhal, F. Herlemont, J. Legrand, A. Fayt, Subdoppler study of the ν_7 band of C_2H_4 with a CO_2 laser sideband spectrometer, Journal of Molecular Spectroscopy 189 (1998) 64 - 73.

[31] J.-M. Flaud, W. J. Lafferty, R. Sams, V. M. Devi, High resolution analysis of the ethylene-1-^{13}C spectrum in the 8.4–14.3-μm region, Journal of Molecular Spectroscopy 259 (2010) 39 - 45.

[32] T. L. Tan, G. B. Lebron, The ν_{12} band of ethylene-1-^{13}C ($^{13}C^{12}CH_4$) by high-resolution FTIR spectroscopy, Journal of Molecular Spectroscopy 261 (2010) 63 - 67.